
Complex-to-Real Random Features for Polynomial Kernels

Jonas Wacker¹ Ruben Ohana^{2,3} Maurizio Filippone¹

Abstract

Kernel methods are ubiquitous in statistical modeling due to their theoretical guarantees as well as their competitive empirical performance. Polynomial kernels are of particular importance as their feature maps model the interactions between the dimensions of the input data. However, the construction time of explicit feature maps scales exponentially with the polynomial degree and a naive application of the kernel trick does not scale to large datasets. In this work, we propose Complex-to-Real (CtR) random features for polynomial kernels that leverage intermediate complex random projections and can yield kernel estimates with much lower variances than their real-valued analogs. The resulting features are real-valued, simple to construct and have the following advantages over the state-of-the-art: 1) shorter construction times, 2) lower kernel approximation errors for commonly used degrees, 3) they enable us to obtain a closed-form expression for their variance.

1. Introduction

Kernel methods offer theoretically principled approaches for nonparametric and nonlinear statistical learning (Scholkopf & Smola, 2002). They often provide statistical guarantees, which makes them the preferred choice when the learning algorithm should behave in an anticipated manner. While kernel methods offer a flexible class of models, their direct application is limited to small datasets as time and memory requirements typically scale at least quadratically in the number of datapoints. Several approaches have been proposed in the past to overcome this bottleneck (e.g., Williams & Seeger 2000; Rahimi & Recht 2007; Rudi et al. 2017).

A particularly important class of kernels are polynomial kernels $k(\mathbf{x}, \mathbf{y}) = (\gamma \mathbf{x}^\top \mathbf{y} + \nu)^p$ for some inputs $\mathbf{x}, \mathbf{y} \in \mathbb{R}^d$, where $\gamma, \nu \geq 0$ and $p \in \mathbb{N}$. Their feature maps can be constructed explicitly and consist of interactions of the

dimensions of \mathbf{x} (or \mathbf{y} respectively) up to order p . Modeling such interactions has proven effective in many applications such as natural language processing (Goldberg & Elhadad, 2008), recommender systems (Rendle, 2010), computer vision (Gao et al. 2016; Fukui et al. 2016) and genomic data analysis (Aschard, 2016). Moreover, more general dot product kernels can be formulated as a positively weighted sum of polynomial kernels through a Taylor expansion, i.e., $k(\mathbf{x}, \mathbf{y}) = \sum_{n=0}^{\infty} a_n (\mathbf{x}^\top \mathbf{y})^n$ with $a_n \geq 0$ (Kar & Karnick, 2012). An extended version of this expansion also exists for the Gaussian kernel (Cotter et al., 2011). One could thus hope to avoid the scalability bottleneck of kernel methods by using explicit feature maps of the polynomial kernel in a parametric model. However, such hopes are dampened since the dimension of these feature maps scales as $\mathcal{O}(d^p)$, which makes their construction practically infeasible as soon as d or p are moderately large.

A solution to this problem are *randomized sketches* (Woodruff, 2014) that linearly project the high-dimensional feature maps of polynomial kernels into a much lower dimensional space (Ahle et al., 2020). The key property of such sketches is that they can be constructed directly from the input data without ever computing the intermediate high-dimensional feature representation of polynomial kernels. Several such approaches have been proposed in the past (Kar & Karnick, 2012; Pham & Pagh, 2013; Hamid et al., 2014; Ahle et al., 2020; Song et al., 2021).

All of these approaches create a *random feature map* $\Phi : \mathbb{R}^d \rightarrow \mathbb{R}^D$, such that the inner product $\Phi(\mathbf{x})^\top \Phi(\mathbf{y})$ of this feature map applied to two different inputs $\mathbf{x}, \mathbf{y} \in \mathbb{R}^d$ is an unbiased estimate of the polynomial kernel, whose variance decreases as D increases. If D is much smaller than the number of datapoints, it becomes cheaper to work with random feature maps than with direct kernel evaluations. This observation connects these sketching methods to random feature methods that were originally proposed for *shift-invariant kernels* by Rahimi & Recht (2007). From now onward, we refer to them as *polynomial sketches*. Notable example applications in which polynomial sketches have been used are fine-grained visual recognition (Gao et al., 2016) and multi-modal visual question answering (Fukui et al., 2016).

In this work, we propose novel *Complex-to-Real (CtR)* polynomial sketches (Section 4.1) that leverage intermediate

¹Department of Data Science, EURECOM, France ²Criteo AI Lab, Paris, France ³Laboratoire de Physique, Ecole Normale Supérieure, France. Correspondence to: Jonas Wacker <jonas.wacker@eurecom.fr>.

complex projections to yield low-variance kernel estimates. The resulting features are real-valued and can be used inside any downstream task without requiring the model to handle complex data, e.g., as a drop-in replacement of the widely known random Fourier features (Rahimi & Recht, 2007).

We derive the variances of CtR-sketches using Gaussian and Rademacher projections in closed form and prove under which conditions they yield lower-variance kernel estimates than comparable sketches in the literature that use only real-valued random projections. These contributions are made in Sections 4.2 and 4.3.

Finally, we propose a novel structured CtR-sketch in Section 5 that is a modified version of TensorSRHT (Ahle et al., 2020). A major contribution of this work is to derive the variance formula of this sketch in closed form while showing empirically in Section 6 under which condition its CtR-extension achieves much lower variances. We compare our novel sketch against TensorSketch (Pham & Pagh, 2013), a state-of-the-art polynomial sketch, for which there is no closed-form variance formula in the literature.¹ We show that CtR-TensorSRHT achieves a large speedup when $D \gg d$. At the same time, it achieves lower kernel approximation errors for moderate $p \leq 5$ that are commonly used in practice.

We made the code used in this work publicly available.²

2. Related Work

Random features for polynomial kernels have been studied for the first time by Kar & Karnick (2012) who propose a **Rademacher sketch** that we revisit in Section 3. The authors further show how general dot product kernels can be approximated using a weighted sum of polynomial sketches.

Pham & Pagh (2013) have proposed **TensorSketch**, a polynomial sketch that is obtained through the convolution of CountSketches (Charikar et al., 2002). TensorSketch achieves lower kernel approximation errors than Rademacher sketches while being significantly faster, i.e., it takes $\mathcal{O}(p(D \log D + d))$ compared to $\mathcal{O}(pdD)$ by leveraging the *Fast Fourier Transform*.

Structured Rademacher polynomial sketches based on the *Subsampled Randomized Hadamard Transform (SRHT)* (Tropp, 2011) have been proposed for the first time by Hamid et al. (2014). A similar sketch has been independently proposed under the name **TensorSRHT** (Ahle et al.,

¹The original paper (Pham & Pagh, 2013) contains a variance formula, but makes the simplifying assumption that TensorSketch has the same variance properties as CountSketch (Charikar et al., 2002) applied to tensorized inputs. A more thorough analysis has been conducted by Avron et al. (2014) who only obtain an upper bound on the variance.

²<https://github.com/joneswack/dp-rfs>

2020), referring to the fact that SRHT is implicitly applied to a tensorized version of the input. Both sketches leverage the Fast Walsh-Hadamard Transform (Fino & Algazi, 1976) for faster projections.

Complex random feature maps have been studied for the linear kernel by Choromanski et al. (2017) and have been generalized to polynomial sketches in Wacker et al. (2022). Unlike the CtR-sketches proposed in this work, the aforementioned polynomial sketches yield complex feature maps and require the downstream model to handle complex data, which can increase computational costs significantly. Ohana et al. (2020) have shown that complex random projections computed by an optical hardware give rise to the approximation of kernels similar to the polynomial kernel.

There exist different algorithms that aim to improve the approximation error of polynomial sketches (Hamid et al., 2014; Ahle et al., 2020; Song et al., 2021). We want to emphasize that the sketches proposed in this work should not be seen as their competitors, but rather as *base sketches* that can directly be used inside all of these algorithms.

A fundamentally different approach are **Spherical Random Features** proposed by Pennington et al. (2015) that require a preprocessing step and produce biased polynomial kernel approximations for data lying on the unit-sphere. We will not discuss this method further in this work.

3. Preliminaries

In this work, we consider polynomial kernels of the form

$$k(\mathbf{x}, \mathbf{y}) = (\gamma \mathbf{x}^\top \mathbf{y} + \nu)^p \quad (1)$$

for some $\mathbf{x}, \mathbf{y} \in \mathbb{R}^d$, where $\gamma, \nu \geq 0$ and $p \in \mathbb{N}$. Both parameters γ and ν can be absorbed by the input vectors by setting $\tilde{\mathbf{x}} := (\sqrt{\gamma} \mathbf{x}^\top, \sqrt{\nu})^\top \in \mathbb{R}^{d+1}$ and $\tilde{\mathbf{y}} := (\sqrt{\gamma} \mathbf{y}^\top, \sqrt{\nu})^\top \in \mathbb{R}^{d+1}$. Therefore, without loss of generality, we assume the kernel to be *homogeneous*, i.e., it can be written as

$$(\gamma \mathbf{x}^\top \mathbf{y} + \nu)^p = (\tilde{\mathbf{x}}^\top \tilde{\mathbf{y}})^p. \quad (2)$$

One can construct explicit features for the polynomial kernel as follows. Let $\mathbf{a} \otimes \mathbf{b} := \text{vec}(\mathbf{a} \mathbf{b}^\top) \in \mathbb{R}^{d^2}$ be the vectorized outer product of two vectors $\mathbf{a}, \mathbf{b} \in \mathbb{R}^d$ and let $\mathbf{a}^{(p)} := \mathbf{a} \otimes \dots \otimes \mathbf{a} \in \mathbb{R}^{d^p}$ be this operation applied p times to a vector with itself. $\tilde{\mathbf{x}}^{(p)}$ then corresponds to the *explicit* feature map of $\tilde{\mathbf{x}}$, i.e., we have $(\tilde{\mathbf{x}}^\top \tilde{\mathbf{y}})^p = (\tilde{\mathbf{x}}^{(p)})^\top \tilde{\mathbf{y}}^{(p)}$ (Scholkopf & Smola, 2002, Proposition 2.1). However, this explicit feature map is $(d+1)^p$ -dimensional and therefore infeasible to construct when d or p are large. This makes randomized sketching an attractive choice.

3.1. Real and Complex-Valued Polynomial Sketches

We study randomized approximations of the polynomial kernel that have originally been proposed by Kar & Karnick

(2012); Hamid et al. (2014). They have been reviewed and generalized to complex projections by Wacker et al. (2022). We revisit these sketches here and present the general complex case that subsumes real polynomial sketches.

Recall that $p \in \mathbb{N}$ is the degree of the polynomial kernel and $D \in \mathbb{N}$ is the projection dimension of the polynomial sketch. We generate $p \times D$ i.i.d. random weights $\mathbf{w}_{i,\ell} \in \mathbb{C}^d$ satisfying $\mathbb{E}[\mathbf{w}_{i,\ell} \overline{\mathbf{w}_{i,\ell}^\top}] = \mathbf{I}_d$ for $i \in \{1, \dots, p\}, \ell \in \{1, \dots, D\}$, where \mathbf{I}_d is the identity matrix of size d . Real-valued example distributions $p(\mathbf{w}_{i,\ell})$ that satisfy this property are the Gaussian distribution $\mathcal{N}(\mathbf{0}, \mathbf{I}_d)$ as well as the Rademacher distribution, i.e., the elements of $\mathbf{w}_{i,\ell}$ are independently sampled from the uniform distribution over $\{1, -1\}$. Their complex-valued analogs are the complex Gaussian distribution $\mathcal{CN}(\mathbf{0}, \mathbf{I}_d)$ and the uniform distribution over $\{1, -1, i, -i\}$ with $i := \sqrt{-1}$.

We define a polynomial sketch $\Phi : \mathbb{R}^d \rightarrow \mathbb{C}^D$ as

$$\Phi(\mathbf{x}) := \frac{1}{\sqrt{D}} \left[\left(\prod_{i=1}^p \mathbf{w}_{i,1}^\top \mathbf{x} \right), \dots, \left(\prod_{i=1}^p \mathbf{w}_{i,D}^\top \mathbf{x} \right) \right]^\top \quad (3)$$

and let $\hat{k}(\mathbf{x}, \mathbf{y}) := \Phi(\mathbf{x})^\top \overline{\Phi(\mathbf{y})} \in \mathbb{C}$ be the approximate kernel for two inputs $\mathbf{x}, \mathbf{y} \in \mathbb{R}^d$, which is unbiased because

$$\mathbb{E}[\hat{k}(\mathbf{x}, \mathbf{y})] = \frac{1}{D} \sum_{\ell=1}^D \prod_{i=1}^p \mathbf{x}^\top \mathbb{E}[\mathbf{w}_{i,\ell} \overline{\mathbf{w}_{i,\ell}^\top}] \mathbf{y} = (\mathbf{x}^\top \mathbf{y})^p.$$

It was shown by Wacker et al. (2022, Theorem 3.3) that polynomial sketches with weights $\mathbf{w}_{i,\ell}$ sampled from the Rademacher distribution are more efficient than Gaussian polynomial sketches and achieve a variance lower bound for the construction in Eq. (3). Hence, we do not consider further example distributions here.

The authors also show that complex Rademacher sketches yield lower variances than real ones when $\sum_{i=1}^d \sum_{j \neq i}^d x_i x_j y_i y_j \geq 0$ holds. This is especially the case for non-negative inputs that appear often in applications of the polynomial kernel, e.g., image data, one-hot encodings, and bag-of-words representations. Otherwise, the inputs can be made positive by min-max feature scaling.

4. Complex-to-Real Polynomial Sketches

Although complex polynomial sketches can yield lower variances than real-valued analogs, they require the downstream model to handle complex data, which can lead to an increased computational cost as we show in Section 6.5. In this section, we introduce *Complex-to-Real (CtR)* polynomial sketches that are real-valued and do not suffer from these problems while being able to achieve much lower variances than real-valued sketches.

Algorithm 1 Complex-to-Real (CtR) Random Features

Input: Datapoint $\mathbf{x} \in \mathbb{R}^d$

Choose projection dimension $D \in \mathbb{N}$, degree $p \in \mathbb{N}$

Sample $\{\mathbf{W}_i\}_{i=1}^p$ with $\mathbf{W}_i \in \mathbb{C}^{D \times d}$ independently according to one of the following sketches:

- Gaussian: $(\mathbf{W}_i)_{\ell,k} \stackrel{i.i.d.}{\sim} \mathcal{CN}(0, 1)$
- Rademacher: $(\mathbf{W}_i)_{\ell,k} \stackrel{i.i.d.}{\sim} \text{Unif}(\{1, -1, i, -i\})$
- TensorSRHT: $\mathbf{W}_i = \mathbf{P}_i \mathbf{H} \mathbf{D}_i$ (see Section 5)

Compute $\Phi_C(\mathbf{x}) := (\mathbf{W}_1 \mathbf{x} \odot \dots \odot \mathbf{W}_p \mathbf{x}) / \sqrt{D}$

Return:

$$\Phi_{\text{CtR}}(\mathbf{x}) := (\text{Re}\{\Phi_C(\mathbf{x})_1\}, \dots, \text{Re}\{\Phi_C(\mathbf{x})_D\}, \text{Im}\{\Phi_C(\mathbf{x})_1\}, \dots, \text{Im}\{\Phi_C(\mathbf{x})_D\})^\top \in \mathbb{R}^{2D}$$

4.1. Transforming Complex into Real Sketches

In the following, we show how to convert complex polynomial sketches into real-valued CtR-sketches. Let $\Phi_C : \mathbb{R}^d \rightarrow \mathbb{C}^D$ be a complex polynomial sketch and $\hat{k}_C(\mathbf{x}, \mathbf{y}) = \Phi_C(\mathbf{x})^\top \overline{\Phi_C(\mathbf{y})}$ the approximate kernel as defined in Section 3.1, where we make the use of complex projections explicit through the subscript C. Let $\text{Re}\{\cdot\}$ and $\text{Im}\{\cdot\}$ denote the real and imaginary parts of a complex vector. $\hat{k}_C(\mathbf{x}, \mathbf{y})$ is generally complex-valued and can hence be written as $\hat{k}_C(\mathbf{x}, \mathbf{y}) = \text{Re}\{\hat{k}_C(\mathbf{x}, \mathbf{y})\} + i \cdot \text{Im}\{\hat{k}_C(\mathbf{x}, \mathbf{y})\}$.

As shown in Section 3.1, $\hat{k}_C(\mathbf{x}, \mathbf{y})$ is unbiased and thus $\mathbb{E}[\hat{k}_C(\mathbf{x}, \mathbf{y})] = k(\mathbf{x}, \mathbf{y}) + 0 \cdot i$. From this it follows that $\mathbb{E}[\text{Re}\{\hat{k}_C(\mathbf{x}, \mathbf{y})\}] = k(\mathbf{x}, \mathbf{y})$ and $\mathbb{E}[\text{Im}\{\hat{k}_C(\mathbf{x}, \mathbf{y})\}] = 0$ through the linearity of the expectation.

We thus define $\hat{k}_{\text{CtR}}(\mathbf{x}, \mathbf{y}) := \text{Re}\{\hat{k}_C(\mathbf{x}, \mathbf{y})\}$ to be our novel kernel estimate which, by expanding the real part of $\Phi_C(\mathbf{x})^\top \overline{\Phi_C(\mathbf{y})}$, can be written as

$$\text{Re}\{\Phi_C(\mathbf{x})\}^\top \text{Re}\{\Phi_C(\mathbf{y})\} + \text{Im}\{\Phi_C(\mathbf{x})\}^\top \text{Im}\{\Phi_C(\mathbf{y})\}.$$

Note that $\text{Re}\{\Phi_C(\mathbf{x})\}, \text{Im}\{\Phi_C(\mathbf{x})\} \in \mathbb{R}^D$, which allows us to define a $2D$ -dimensional *real-valued* polynomial sketch

$$\Phi_{\text{CtR}}(\mathbf{x}) := (\text{Re}\{\Phi_C(\mathbf{x})_1\}, \dots, \text{Re}\{\Phi_C(\mathbf{x})_D\}, \text{Im}\{\Phi_C(\mathbf{x})_1\}, \dots, \text{Im}\{\Phi_C(\mathbf{x})_D\})^\top \in \mathbb{R}^{2D}, \quad (4)$$

for which we have

$$\Phi_{\text{CtR}}(\mathbf{x})^\top \Phi_{\text{CtR}}(\mathbf{y}) = \text{Re}\{\hat{k}_C(\mathbf{x}, \mathbf{y})\} = \hat{k}_{\text{CtR}}(\mathbf{x}, \mathbf{y}). \quad (5)$$

We call Φ_{CtR} a *Complex-to-Real (CtR)* polynomial sketch and summarize its construction in Alg. (1).

4.2. Variances of Complex-to-Real Polynomial Sketches

Our major contribution of this section is to derive the variance formulas of Gaussian and Rademacher CtR polynomial

sketches. In Section A.1, we show that CtR-sketches generally have the following variance structure:

$$\mathbb{V}[\hat{k}_{\text{CtR}}(\mathbf{x}, \mathbf{y})] = \frac{1}{2} \left(\mathbb{V}[\hat{k}_{\text{C}}(\mathbf{x}, \mathbf{y})] + \mathbb{P}\mathbb{V}[\hat{k}_{\text{C}}(\mathbf{x}, \mathbf{y})] \right) \quad (6)$$

$$\text{with } \mathbb{P}\mathbb{V}[\hat{k}_{\text{C}}(\mathbf{x}, \mathbf{y})] := \mathbb{E}[\hat{k}_{\text{C}}(\mathbf{x}, \mathbf{y})^2] - (\mathbf{x}^\top \mathbf{y})^{2p}$$

being the *pseudo-variance* of $\hat{k}_{\text{C}}(\mathbf{x}, \mathbf{y})$ and $\mathbb{V}[\hat{k}_{\text{C}}(\mathbf{x}, \mathbf{y})]$ its variance. We derive $\mathbb{V}[\hat{k}_{\text{C}}(\mathbf{x}, \mathbf{y})]$ and $\mathbb{P}\mathbb{V}[\hat{k}_{\text{C}}(\mathbf{x}, \mathbf{y})]$ for Gaussian and Rademacher sketches in Section A.2 and summarize these results in Table (1). TensorSRHT will be covered in detail in Section 5, but we already add its variance and pseudo-variance derived in Section B.2 for completeness. For a direct comparison, we add the variances of real polynomial sketches Φ_{R} to Table (1) that do not use complex random projections as shown in Section 3.1.

The dimension of the feature map Φ_{CtR} (4) is $2D$ for a given D random samples, while the dimension of Φ_{R} (3) is only D . Feature maps with higher dimensions usually render the downstream task more expensive. The key question that we address in this work is thus: Does the CtR estimator in Eq. (5) yield lower variances as $\hat{k}_{\text{R}}(\mathbf{x}, \mathbf{y}) = \Phi_{\text{R}}(\mathbf{x})^\top \Phi_{\text{R}}(\mathbf{y})$ if Φ_{CtR} and Φ_{R} have the *same* output dimension? We will show in Section 4.3 that this is indeed the case.

4.3. Variance Reduction of CtR-Sketches

We begin by studying the variance reduction properties of Rademacher and Gaussian CtR-sketches over their real-valued analogs that were originally proposed by (Kar & Karnick, 2012; Hamid et al., 2014). Let $\Phi_{\text{R}} : \mathbb{R}^d \rightarrow \mathbb{R}^{2D}$ (using $2D$ random features) be a real polynomial sketch as defined in Section 3.1 and $\Phi_{\text{CtR}} : \mathbb{R}^d \rightarrow \mathbb{R}^{2D}$ a CtR-sketch (using only D random features) as defined in Eq. (4). Let $\hat{k}_{\text{R}}(\mathbf{x}, \mathbf{y})$ and $\hat{k}_{\text{CtR}}(\mathbf{x}, \mathbf{y})$ be the respective approximate kernels for some $\mathbf{x}, \mathbf{y} \in \mathbb{R}^d$. Then we can provide the following theorem for the case of Rademacher sketches.

Theorem 4.1 (CtR-Rademacher advantage) *Let $a := \sum_{i=1}^d \sum_{j \neq i}^d x_i x_j y_i y_j$ and $b(j) := \|\mathbf{x}\|^{2j} \|\mathbf{y}\|^{2j} - (\sum_{i=1}^d x_i^2 y_i^2)^j \geq 0$. Then $\mathbb{V}[\hat{k}_{\text{RtC}}(\mathbf{x}, \mathbf{y})] - \mathbb{V}[\hat{k}_{\text{R}}(\mathbf{x}, \mathbf{y})]$ yields*

$$\frac{1}{2D} \sum_{k=2}^p \sum_{j=0}^{k-1} \binom{p}{k} \binom{k}{j} b(j) a^{p-j} \geq 0 \quad \text{if } a \geq 0.$$

Furthermore, CtR-Rademacher sketches achieve the lowest possible variance for $\hat{k}_{\text{CtR}}(\mathbf{x}, \mathbf{y}) = \text{Re}\{\Phi_{\text{C}}(\mathbf{x})^\top \overline{\Phi_{\text{C}}(\mathbf{y})}\}$ with Φ_{C} being defined through Eq. (3).

Proof The variance reduction property is proven in Section A.3.2 and the lowest CtR-variance property is proven in Section A.2. ■

The theorem tells us that Φ_{CtR} should be preferred over Φ_{R} when $a \geq 0$ for two given inputs $\mathbf{x}, \mathbf{y} \in \mathbb{R}^d$ and the variance gap increases as p increases. This is the same condition under which complex Rademacher sketches have lower variances than real ones (see Section 3.1), which holds, e.g., when \mathbf{x}, \mathbf{y} are non-negative. Even when this condition is not always met, CtR-Rademacher sketches perform similar or better than real ones in our experiments in Fig. 5.

We can additionally provide the following theorem for Gaussian polynomial sketches proved in Section A.3.1.

Theorem 4.2 (CtR-Gaussian advantage) *For any $\mathbf{x}, \mathbf{y} \in \mathbb{R}^d$, $\mathbb{V}[\hat{k}_{\text{RtC}}(\mathbf{x}, \mathbf{y})] - \mathbb{V}[\hat{k}_{\text{R}}(\mathbf{x}, \mathbf{y})]$ yields*

$$\frac{1}{2D} \sum_{k=0}^{p-1} \binom{p}{k} (2^k - 1) (\mathbf{x}^\top \mathbf{y})^{2k} \left(\|\mathbf{x}\|^2 \|\mathbf{y}\|^2 \right)^{p-k} \geq 0.$$

Thus, regardless of the input data, Φ_{CtR} should be preferred over Φ_{R} when using Gaussian polynomial sketches. The advantage again increases with p .

The origin of the variance reduction. We provide an alternative derivation of $\mathbb{V}[\hat{k}_{\text{CtR}}(\mathbf{x}, \mathbf{y})]$ for the case of Gaussian polynomial sketches with $p = 2$ in Section A.3.3. Unlike the kernel estimate obtained through real polynomial sketches, the approximate kernel $\hat{k}_{\text{CtR}}(\mathbf{x}, \mathbf{y})$ yields a *sum* of correlated products and the overall variance reduction is due to two mixed effects: 1) each addend of the sum is downscaled by the factor 2^p because the real and imaginary parts of $w_{i,\ell} \sim \mathcal{CN}(\mathbf{0}, \mathbf{I}_d)$ in Eq. (3) have a variance of $\frac{1}{2}$, 2) the downscaled covariances and variances of the addends are mostly either zero or have small values such that their addition does not outweigh the downscaling effect. We refer the reader to Section A.3.4 for a detailed explanation.

5. Structured Rademacher Sketches

In this section, we propose a novel structured Rademacher sketch and derive its variance in closed form, which is the major contribution of this section. At the same time, we embed this sketch into our CtR-framework and evaluate its CtR-advantage empirically in Section 6. Our sketch is a slightly modified version³ of TensorSRHT (Ahle et al., 2020). TensorSRHT achieves its fast projections through structured Hadamard matrices that we introduce next.

Hadamard matrices. Let $n := 2^m$ with $m \in \mathbb{N}$, and denote $\mathbf{H}_n \in \{1, -1\}^{n \times n}$ as the unnormalized Hadamard

³We refer the reader to Section B.1 for a detailed explanation of the subtle differences. There is no closed form variance for the TensorSRHT sketch by Ahle et al. (2020) in the literature.

Table 1. Variances of complex $\hat{k}_C(\mathbf{x}, \mathbf{y})$ and real $\hat{k}_R(\mathbf{x}, \mathbf{y})$ as well as pseudo-variances of complex $\hat{k}_C(\mathbf{x}, \mathbf{y})$ are shown. $\mathbb{V}_{\text{Rad.}}^{(p)}$, $\mathbb{V}_{\text{Rad.}}^{(1)}$ and $\mathbb{P}\mathbb{V}_{\text{Rad.}}^{(p)}$, $\mathbb{P}\mathbb{V}_{\text{Rad.}}^{(1)}$ are the Rademacher variances and pseudo-variances for a given degree p and $p = 1$, respectively.

Sketch	Variance $\mathbb{V}[\hat{k}_C(\mathbf{x}, \mathbf{y})]$ ($q = 1$) and $\mathbb{V}[\hat{k}_R(\mathbf{x}, \mathbf{y})]$ ($q = 2$)	Pseudo-Variance $\mathbb{P}\mathbb{V}[\hat{k}_C(\mathbf{x}, \mathbf{y})]$
Gaussian	$D^{-1}[(\ \mathbf{x}\ ^2 \ \mathbf{y}\ ^2 + q(\mathbf{x}^\top \mathbf{y})^2)^p - (\mathbf{x}^\top \mathbf{y})^{2p}]$	$D^{-1}[(2(\mathbf{x}^\top \mathbf{y})^2)^p - (\mathbf{x}^\top \mathbf{y})^{2p}]$
Rademacher	$D^{-1}[(\ \mathbf{x}\ ^2 \ \mathbf{y}\ ^2 + q((\mathbf{x}^\top \mathbf{y})^2 - \sum_{i=1}^d x_i^2 y_i^2))^p - (\mathbf{x}^\top \mathbf{y})^{2p}]$	$D^{-1}[(2(\mathbf{x}^\top \mathbf{y})^2 - \sum_{i=1}^d x_i^2 y_i^2)^p - (\mathbf{x}^\top \mathbf{y})^{2p}]$
TensorSRHT	$\mathbb{V}_{\text{Rad.}}^{(p)} - (1 - 1/D) \cdot [(\mathbf{x}^\top \mathbf{y})^{2p} - (\text{CVar.})^p]$ $\text{CVar.} = (\mathbf{x}^\top \mathbf{y})^2 - (\lceil D/d \rceil d - 1)^{-1} \mathbb{V}_{\text{Rad.}}^{(1)}$	$\mathbb{P}\mathbb{V}_{\text{Rad.}}^{(p)} - (1 - 1/D) \cdot [(\mathbf{x}^\top \mathbf{y})^{2p} - (\text{CPVar.})^p]$ $\text{CPVar.} = (\mathbf{x}^\top \mathbf{y})^2 - (\lceil D/d \rceil d - 1)^{-1} \mathbb{P}\mathbb{V}_{\text{Rad.}}^{(1)}$

matrix, which is recursively defined as

$$\mathbf{H}_{2n} := \begin{bmatrix} \mathbf{H}_n & \mathbf{H}_n \\ \mathbf{H}_n & -\mathbf{H}_n \end{bmatrix}, \quad \text{with} \quad \mathbf{H}_2 := \begin{bmatrix} 1 & 1 \\ 1 & -1 \end{bmatrix}.$$

From now onward, we always use $\mathbf{H}_d \in \{1, -1\}^{d \times d}$ with d being the dimension of the input vectors, assuming $d = 2^m$ for some $m \in \mathbb{N}$. If $d \neq 2^m$ for any m , we pad the input vectors with 0 until their dimension becomes 2^m for some m . We have $\mathbf{H}_d \mathbf{H}_d^\top = \mathbf{H}_d^\top \mathbf{H}_d = d\mathbf{I}_d$ and the recursive definition of \mathbf{H}_d gives rise to the Fast Walsh-Hadamard transform (Fino & Algazi, 1976) that multiplies \mathbf{H}_d with a vector $\mathbf{a} \in \mathbb{R}^d$ in $\mathcal{O}(d \log d)$ instead of $\mathcal{O}(d^2)$ time while the matrix \mathbf{H}_d does not need to be stored in memory. We drop the subscript d from now for ease of presentation.

5.1. Our Version of TensorSRHT

We now introduce our version of *TensorSRHT* and present the general complex case that subsumes the real case.

Random variables. We define a set of *Rademacher vectors* $\{\mathbf{d}_i\}_{i=1}^p$ with $\mathbf{d}_i \in \mathbb{C}^d$ whose elements are independently and uniformly sampled from $\{1, -1\}$ (real case) and from $\{1, -1, i, -i\}$ (complex case). We further write $\mathbf{D}_i := \text{diag}(\mathbf{d}_i)$, where $\text{diag}(\mathbf{d}_i) \in \mathbb{C}^{d \times d}$ denotes a diagonal matrix with the vector \mathbf{d}_i being its diagonal elements.

Next, we create a set of *random sampling matrices*. For this purpose, we concatenate the index vector $(1, \dots, d)^\top \in \mathbb{R}^d$ a total number of $\lceil D/d \rceil$ times with itself and call the resulting vector $\mathbf{p}_{\text{base}} \in \mathbb{R}^{\lceil D/d \rceil d}$, where $\lceil D/d \rceil$ rounds up D/d to the next integer. We then shuffle the elements of \mathbf{p}_{base} for each $i \in \{1, \dots, p\}$ independently at random and call the shuffled vectors $\{\mathbf{p}_i\}_{i=1}^p$. Each vector \mathbf{p}_i defines a sampling matrix $\mathbf{P}_i = (\mathbf{e}_{p_{i,1}}, \dots, \mathbf{e}_{p_{i,D}})^\top \in \mathbb{R}^{D \times d}$, where $\mathbf{e}_{p_{i,\ell}} \in \mathbb{R}^d$ is a vector whose element $p_{i,\ell}$ is equal to one and all other elements are zero. We keep only the first D elements of every \mathbf{p}_i to create D random feature samples.

Sketch construction. We define the projections $\phi_i(\mathbf{x}) := \mathbf{P}_i \mathbf{H} \mathbf{D}_i \mathbf{x}$ for every $i \in \{1, \dots, p\}$. Let $\mathbf{a} \odot \mathbf{b}$ denote the element-wise product between two vectors $\mathbf{a}, \mathbf{b} \in \mathbb{R}^d$. The multiplication $\mathbf{D}_i \mathbf{x}$ can then be written as $\mathbf{d}_i \odot \mathbf{x}$

and thus be achieved in $\mathcal{O}(d)$ time. The multiplication by \mathbf{H} takes $\mathcal{O}(d \log d)$ as mentioned before and applying the sampling matrix \mathbf{P}_i takes $\mathcal{O}(D)$ time because \mathbf{P}_i has only D non-zero elements. Computing all $\{\phi_i(\mathbf{x})\}_{i=1}^p$ thus takes $\mathcal{O}(p(d \log d + D))$. We define the final sketch $\Phi(\mathbf{x}) := (\phi_1(\mathbf{x}) \odot \dots \odot \phi_p(\mathbf{x})) / \sqrt{D}$, which costs an additional $\mathcal{O}(pD)$ time and hence does not change the aforementioned overall time complexity.

In fact, we can rewrite our sketch using Eq. (3) making it closely related to Rademacher polynomial sketches. Let $\mathbf{W}_i := \mathbf{P}_i \mathbf{H} \mathbf{D}_i \in \mathbb{C}^{D \times d}$ and define $\mathbf{h}_{p_{i,\ell}}^\top$ to be the $p_{i,\ell}$ -th row of \mathbf{H} . We can refer to the ℓ -th row of \mathbf{W}_i as $\mathbf{w}_{i,\ell}^\top := \mathbf{h}_{p_{i,\ell}}^\top \odot \mathbf{d}_i^\top$ and use $\mathbf{w}_{i,\ell}^\top$ directly inside Eq. (3). A CtR-extension of TensorSRHT is constructed in the same way as for the other sketches introduced before (see Section 4.1). We show this in Alg. (1) for a simple implementation.

The unbiasedness of our novel sketch is easy to show. Although the $\{\mathbf{w}_{i,\ell}\}_{\ell=1}^D$ are statistically dependent between each other through \mathbf{d}_i , the elements inside a single row $\mathbf{w}_{i,\ell}^\top$ are independent samples uniformly drawn from $\{1, -1\}$ (real case) and $\{1, -1, i, -i\}$ (complex case). Therefore, we have $\mathbb{E}[\mathbf{w}_{i,\ell} \overline{\mathbf{w}_{i,\ell}}^\top] = \mathbf{I}_d$ and thus satisfy the unbiasedness criterion in Section 3.1.

5.2. The Variance of CtR-TensorSRHT

A major contribution of this work is to derive the variance of our proposed CtR-TensorSRHT sketch in closed form, which requires the derivation of the variance and pseudo-variance of complex TensorSRHT as shown in Eq. (6). They are derived in Section B.2 and we summarize them in Table (1). We also derive the variance of real TensorSRHT in Section B.2.2 and add it to Table (1) for comparison.

TensorSRHT can yield lower variances than Rademacher polynomial sketches as it removes the i.i.d. constraint between the $\{\mathbf{w}_{i,\ell}\}_{\ell=1}^D$ in Eq. (3). In fact, these vectors are mutually orthogonal for two $\ell \neq \ell'$ when $\mathbf{h}_{p_{i,\ell}} \neq \mathbf{h}_{p_{i,\ell'}}$ since $\mathbf{h}_{p_{i,\ell}}$ and $\mathbf{h}_{p_{i,\ell'}}$ are orthogonal. This dependence introduces the reduction term

$$\mathbb{V}_{\text{Var.}/\text{PVar.}} := (1 - 1/D)[(\mathbf{x}^\top \mathbf{y})^{2p} - (\text{CVar.}/\text{PVar.})^p]$$

that is subtracted from the original Rademacher variance $\mathbb{V}_{\text{Rad.}}^{(p)}$ and pseudo-variance $\mathbb{P}\mathbb{V}_{\text{Rad.}}^{(p)}$, respectively as shown in Table (1), where we also define $C_{\text{Var.}}$ and $C_{\text{PVar.}}$.

If p is odd, $(C_{\text{Var.}})^p \leq (\mathbf{x}^\top \mathbf{y})^{2p}$ because $\mathbb{V}_{\text{Rad.}}^{(1)} \geq 0$ and therefore $R_{\text{Var.}} \geq 0$ holds. In this case, the variance of complex/real TensorSRHT is upper-bounded by the complex/real Rademacher variance $\mathbb{V}_{\text{Rad.}}^{(p)} \geq 0$.

If we further have $\mathbb{P}\mathbb{V}_{\text{Rad.}}^{(1)} = \sum_{i=1}^d \sum_{j \neq i}^d x_i x_j y_i y_j \geq 0$, the pseudo-variance of complex TensorSRHT is also upper-bounded by the Rademacher pseudo-variance. This is because $0 \leq (C_{\text{PVar.}})^p \leq (\mathbf{x}^\top \mathbf{y})^{2p}$ and $R_{\text{PVar.}} \geq 0$ hold.

As both the variance and the pseudo-variance of complex TensorSRHT are upper-bounded by the ones of complex Rademacher sketches under the above conditions, CtR-TensorSRHT is guaranteed to have a lower variance than CtR-Rademacher through Eq. (6) in this case. Moreover, CtR-TensorSRHT inherits the variance reduction of CtR-Rademacher sketches over their real analogs because the Rademacher variance and pseudo-variance are both included in the ones of complex TensorSRHT (see Table (1)). In the next section, we carry out an empirical comparison of CtR-TensorSRHT against its real-valued analog and see later on that it yields better kernel approximations than Gaussian and Rademacher sketches while being significantly faster.

6. Experiments

In this section, we carry out a systematic comparison of the CtR polynomial sketches discussed in this work against their real-valued analogs as well as TensorSketch (Pham & Pagh, 2013), a state-of-the-art polynomial sketch.

6.1. Experimental Setup

We start by describing the datasets as well as the target kernel that we approximate through polynomial sketches.

Datasets. We use the same four datasets throughout: Letter and Mocap (Dua & Graff, 2017), CIFAR-10⁴ (Krizhevsky et al., 2009) and MNIST (Lecun et al., 1998). All datasets except for Mocap contain only non-negative inputs. For Mocap, we subtract the minimum value of each input dimension $\{x_i\}_{i=1}^d$ of $\mathbf{x} \in \mathbb{R}^d$ across the dataset to achieve non-negativity.

Target kernel and its approximation. The target polynomial kernel is always $k(\mathbf{x}, \mathbf{y}) = (\mathbf{x}^\top \mathbf{y} + 1)^p$ and we unit-normalize the data unless otherwise specified to make the kernel bounded and improve numerical stability. Further results for differently scaled data as well as optimized kernel

⁴We use the the convolutional outputs of a pretrained ResNet34 (He et al., 2016) on ImageNet (Russakovsky et al., 2015).

parameters are contained in Section C. Since CtR polynomial sketches Φ_{CtR} are $2D$ -dimensional when sampling D random features, we compare them against real-valued polynomial sketches Φ_{R} with $2D$ random features to obtain the *same* dimension of the feature map. We measure kernel approximation quality through the relative Frobenius norm error in Fig. (2) and (3), which is defined as $\|\hat{\mathbf{K}} - \mathbf{K}\|_F / \|\mathbf{K}\|_F$, where $\hat{\mathbf{K}}$ is the random feature approximation of the exact kernel matrix \mathbf{K} with $K_{ij} = k(\mathbf{x}_i, \mathbf{x}_j)$ and $\mathbf{x}_i, \mathbf{x}_j \in X_{*,\text{sub}}$. $X_{*,\text{sub}}$ is a subset of the test data of size $N_{*,\text{sub}} = 1000$ of each dataset that is resampled for 100 different seeds used in these experiments. We use a 90/10 train/test split for Letter and Mocap that is recomputed for every seed, while it is provided for CIFAR-10 and MNIST.

All time benchmarks are run on an NVIDIA P100 GPU and PyTorch 1.10 (Paszke et al., 2019).

6.2. Variance Comparison of CtR-TensorSRHT

We carry out a variance comparison for CtR-TensorSRHT and its real-valued analog (see Section 5). For Rademacher and Gaussian sketches, this comparison is provided by Theorems 4.1 and 4.2 and an empirical comparison for the Rademacher case is shown in Fig. (5) in Section C.1.

Comparison against real TensorSRHT. Since we obtained the variances of CtR-TensorSRHT and real TensorSRHT in closed form in Section 5, we can evaluate their variance ratio on our datasets. Fig. (1a) shows this comparison through empirical cumulative distribution functions of the variance ratios evaluated on all input pairs inside 1000 random samples of each dataset. We observe that CtR-TensorSRHT outperforms real TensorSRHT (all variance ratios < 1) and the improvement increases with p .

As the variance of TensorSRHT is closely related to Rademacher variances as shown in Section 5, we study the importance of the non-negativity condition of the data in Theorem 4.1 for CtR-TensorSRHT. For this purpose, we repeat the same experiment as before for zero-centered data that breaks the non-negativity condition. Results are shown in Fig. (6a) in Section C.1. We see that CtR-TensorSRHT performs similarly as its real analog in this case. Therefore, a variance reduction happens in particular for non-negative data as is the case for CtR-Rademacher sketches.

Comparison against TensorSketch. We repeat the same experiment as before and evaluate the variance ratios of CtR-TensorSRHT against TensorSketch. As the variance of TensorSketch is not available in closed form, we estimate it using 1000 Monte-Carlo samples of the kernel estimate. Figure (1b) shows a comparison of the variance ratios. In general, CtR-TensorSRHT improves over TensorSketch for $p \leq 5$ (more than half of the ratios are less than one). This is

an important advantage as such degrees are commonly used in practice (Pham & Pagh, 2013; Gao et al., 2016; Fukui et al., 2016). For $p = 1$, TensorSRHT always has a variance of zero as soon as $D = kd$ for $k \in \mathbb{N}$, which can be derived from the TensorSRHT variance equation in Table (1).

For large p , TensorSketch and CtR-TensorSRHT perform similarly well (around half the variance ratios are smaller/greater than 1) except for some cases with low-dimensional data where TensorSketch performs better. The ratios would be much worse if we used the real TensorSRHT instead as shown in Fig. (6b) in Section C.1, which underlines the relative improvement of the CtR-extension.

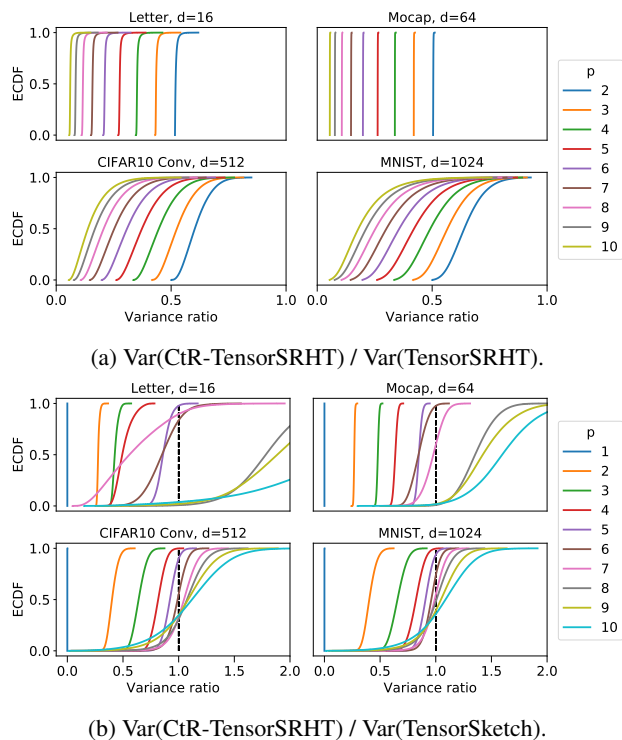


Figure 1. Empirical cumulative distribution function of variance ratios for feature maps with equal dimension $D = 2d$. The target kernel is $(\mathbf{x}^\top \mathbf{y} + 1)^p$.

6.3. Feature Construction Time Comparison

In the following, we carry out a feature construction time comparison of the methods presented in this work against TensorSketch that has a time complexity $\mathcal{O}(p(D \log D + D))$. Recall that our proposed TensorSRHT approach in Section 5 has a time complexity of $\mathcal{O}(p(d \log d + D))$ and is thus faster in theory when $D > d$. The left plot in Fig. (2) shows that this is also the case in practice.

The construction times of real TensorSRHT and CtR-TensorSRHT have a smaller slope with respect to D than the other sketches leading to the lowest feature construction

times, in particular when $D \gg d$. There is a small computational overhead for CtR-TensorSRHT compared to real TensorSRHT because CtR-TensorSRHT initially requires two Hadamard-projections (real and imaginary parts), but uses the same sampling matrix leading to the same scaling property with respect to D .

The right plot of Fig. (2) shows the kernel approximation error (rel. Frobenius norm error) under a computational budget. We can see that our proposed CtR-TensorSRHT gives the best kernel approximations in the shortest amount of time when D is sufficiently large.

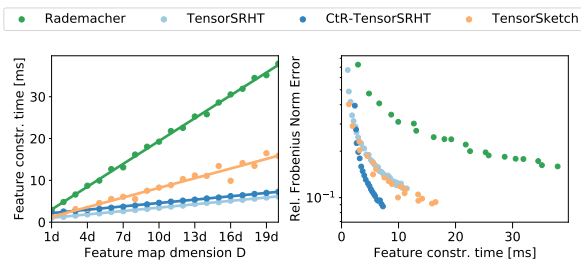


Figure 2. (Left) Feature construction time against feature map dimension D . (Right) Kernel approximation error (rel. Frobenius norm error) against feature construction time. We approximate the kernel $k(\mathbf{x}, \mathbf{y}) = (\mathbf{x}^\top \mathbf{y} + 1)^6$ on 1000 random MNIST samples.

6.4. Kernel Approximation and GP Classification

In this section, we compare the sketches discussed in this work for the downstream task of Gaussian Process (GP) classification. We model GP classification as a multi-class GP regression problem with transformed labels (Milios et al., 2018) for which we obtain closed-form solutions. We use a fixed polynomial kernel $(\mathbf{x}^\top \mathbf{y} + 1)^3$ to measure the effects of the random feature approximations in isolation without needing to verify the convergence of iterative solvers⁵. To measure the convergence towards a target GP when using random features, we use the Kullback-Leibler (KL) divergence between the GP predictive distribution using the approximate kernel and the predictive distribution using the target kernel. These distributions are evaluated on the test data and the GPs are trained on a random subset of size 5000 of the training data as the reference GP cannot be scaled to a large number of datapoints. Classification errors are obtained using the whole training and test data instead.

Fig. (3) shows the results of this comparison as well as associated kernel approximation errors (Rel. Frob. Error) on a random subset of the test data for each seed. As shown in Fig. (1b), CtR-TensorSRHT has a lower variance than Ten-

⁵The kernel parameters are a standard choice used in, e.g., *scikit-learn* (Pedregosa et al., 2011). Consult Fig. (8) for an experiment where we optimize the hyperparameters instead.

sorSketch for $p = 3$, which is reflected in the corresponding kernel approximation errors in Fig. (3). These errors are the lowest for CtR-TensorSRHT and also fluctuate the least. TensorSRHT thus performs better than unstructured Gaussian and Rademacher sketches as discussed in Section 5. The CtR extension makes TensorSRHT perform similarly on the downstream task of GP classification as TensorSketch (similar KL-divergence and classification error). The results are worse for TensorSRHT without the CtR-extension.

We add a CtR-modification of TensorSketch⁶ to our comparison. This modification does not yield any improvements in our experiments confirming that CtR-sketches are only beneficial for the feature construction in Eq. (3).

Experiments on further datasets and different scalings of the data in Section C.3 yield similar results. The relative improvement of CtR-sketches over their real-valued analogs *increases* for kernel approximations *and* downstream task when p becomes larger as shown in Fig. (11).

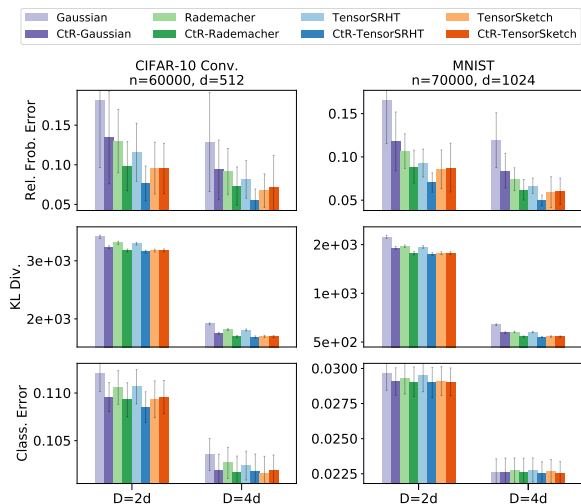


Figure 3. Gaussian Process classification experiments comparing different polynomial sketches along with their CtR extensions for $D \in \{2d, 4d\}$. The target polynomial kernel is $k(\mathbf{x}, \mathbf{y}) = (\mathbf{x}^\top \mathbf{y} + 1)^3$. Means and std. devs. are computed on 100 seeds.

6.5. Comparing Real, Complex and CtR-Sketches

Lastly, we compare the convergence of a GP classifier using real, complex and CtR-TensorSRHT towards one using the exact kernel on MNIST under a given time budget in Fig. (4). We can see that a complex GP classifier using complex TensorSRHT needs roughly the same time for a projection dimension D as real and CtR-TensorSRHT for dimension

⁶We replace sign hash function $s : [d] \rightarrow \{1, -1\}$ with $s : [d] \rightarrow \{1, -1, i, -i\}$ in (Pham & Pagh, 2013, Def. 1) giving rise to a complex-valued TensorSketch.

$2D$. This gives a clear advantage to the CtR-TensorSRHT sketch that achieves the lowest KL-divergence and test errors in the same amount of time. Therefore, we recommend the use of CtR-TensorSRHT over real and complex TensorSRHT.

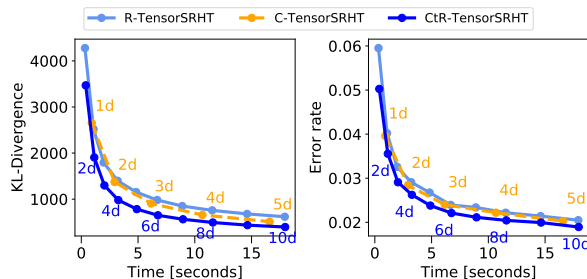


Figure 4. KL-divergence (left) and test error (right) for a given computation time budget computed on MNIST ($d = 1024$). Projection dimensions are annotated next to the respective measurements.

7. Conclusion

In this work, we introduced *Complex-to-Real (CtR)* polynomial sketches, derived their variances in closed form and showed that they can lead to substantial variance improvements compared to real-valued analogs used in the literature. Most notably, we derived a novel CtR-TensorSRHT sketch that yields lower kernel approximation errors than the state-of-the-art for moderate $p \leq 5$ (commonly used in practice). At the same time, it is faster when $D > d$.

We showed that our CtR-framework achieves variance reductions through a downscaled sum of correlated random variables (see Section A.3.4). Building on this observation, we aim to develop further sketches with a more optimal covariance structure.

Regarding practical applications, our sketches can be easily integrated into deep learning models, as they are real-valued. Example applications are Deep Gaussian Processes by Cutajar et al. (2017) and bilinear convolutional neural networks (Gao et al., 2016; Fukui et al., 2016) that heavily rely on random feature maps. They would thus benefit from the speedup of CtR-TensorSRHT over TensorSketch as we already show for a shallow GP model in Fig. (8).

Another application for our sketches is unsupervised learning. In Section C.4, we conduct experiments showing the superiority of polynomial sketches for the approximation of the *Kernel Inception Distance* (Bińkowski et al., 2018) compared to commonly used methods. These promising results warrant a further application of CtR polynomial sketches in other areas of unsupervised learning such as statistical hypothesis testing using kernels (Gretton et al., 2012).

Acknowledgements

We thank Motonobu Kanagawa for helpful discussions. MF gratefully acknowledges support from the AXA Research Fund and the Agence Nationale de la Recherche (grant ANR-18-CE46-0002 and ANR-19-P3IA-0002). RO acknowledges support from Région Ile-de-France.

References

- Ahle, T. D., Kapralov, M., Knudsen, J. B. T., Pagh, R., Velinger, A., Woodruff, D. P., and Zandieh, A. Oblivious sketching of high-degree polynomial kernels. In *Proceedings of the Thirty-First Annual ACM-SIAM Symposium on Discrete Algorithms*, pp. 141–160. Society for Industrial and Applied Mathematics, 2020.
- Aschard, H. A perspective on interaction effects in genetic association studies. *Genetic epidemiology*, 40(8): 678–688, 2016.
- Avron, H., Nguyen, H. L., and Woodruff, D. P. Subspace embeddings for the polynomial kernel. In *Advances in Neural Information Processing Systems 27*, pp. 2258–2266. Curran Associates, Inc., 2014.
- Bińkowski, M., Sutherland, D. J., Arbel, M., and Gretton, A. Demystifying MMD GANs. In *International Conference on Learning Representations*, 2018. URL <https://openreview.net/forum?id=r1lUOzWCW>.
- Charikar, M., Chen, K., and Farach-Colton, M. Finding frequent items in data streams. In *Proceedings of the 29th International Colloquium on Automata, Languages and Programming*, pp. 693–703. Springer-Verlag, 2002.
- Choromanski, K., Rowland, M., and Weller, A. The unreasonable effectiveness of structured random orthogonal embeddings. In *Advances in Neural Information Processing Systems 31*, pp. 218–227. Curran Associates Inc., 2017.
- Cotter, A., Keshet, J., and Srebro, N. Explicit approximations of the gaussian kernel. *CoRR*, abs/1109.4603, 2011.
- Cutajar, K., Bonilla, E. V., Michiardi, P., and Filippone, M. Random feature expansions for deep Gaussian processes. In *Proceedings of the 34th International Conference on Machine Learning*, volume 70 of *Proceedings of Machine Learning Research*, pp. 884–893. PMLR, 2017.
- Dua, D. and Graff, C. UCI machine learning repository, 2017. URL <http://archive.ics.uci.edu/ml>.
- Fino, B. J. and Algazi, V. R. Unified matrix treatment of the fast walsh-hadamard transform. *IEEE Transactions on Computers*, 25(11):1142–1146, 1976.
- Fukui, A., Park, D. H., Yang, D., Rohrbach, A., Darrell, T., and Rohrbach, M. Multimodal compact bilinear pooling for visual question answering and visual grounding. In *Proceedings of the 2016 Conference on Empirical Methods in Natural Language Processing*, pp. 457–468. Association for Computational Linguistics, 2016.
- Gao, Y., Beijbom, O., Zhang, N., and Darrell, T. Compact bilinear pooling. *Proceedings of the 2016 IEEE Computer Society Conference on Computer Vision and Pattern Recognition*, pp. 317–326, 2016.
- Goldberg, Y. and Elhadad, M. splitsvm: Fast, space-efficient, non-heuristic, polynomial kernel computation for NLP applications. In *Proceedings of the 46th Annual Meeting of the Association for Computational Linguistics*, pp. 237–240. The Association for Computer Linguistics, 2008.
- Gretton, A., Borgwardt, K. M., Rasch, M. J., Schölkopf, B., and Smola, A. A kernel two-sample test. *Journal of Machine Learning Research*, 13(25):723–773, 2012.
- Hamid, R., Xiao, Y., Gittens, A., and DeCoste, D. Compact random feature maps. In *Proceedings of the 31th International Conference on Machine Learning*, volume 32 of *Proceedings of Machine Learning Research*, pp. 19–27. PMLR, 2014.
- He, K., Zhang, X., Ren, S., and Sun, J. Deep residual learning for image recognition. In *2016 IEEE Conference on Computer Vision and Pattern Recognition*, pp. 770–778, 2016.
- Kar, P. and Karnick, H. Random feature maps for dot product kernels. In *Proceedings of the Fifteenth International Conference on Artificial Intelligence and Statistics*, volume 22 of *JMLR Proceedings*, pp. 583–591. JMLR, 2012.
- Krizhevsky, A., Hinton, G., et al. Learning multiple layers of features from tiny images. 2009.
- Lecun, Y., Bottou, L., Bengio, Y., and Haffner, P. Gradient-based learning applied to document recognition. *Proceedings of the IEEE*, 86(11):2278–2324, 1998.
- Milios, D., Camoriano, R., Michiardi, P., Rosasco, L., and Filippone, M. Dirichlet-based gaussian processes for large-scale calibrated classification. In *Advances in Neural Information Processing Systems 31*, pp. 6008–6018. Curran Associates, Inc., 2018.
- Ohana, R., Wacker, J., Dong, J., Marmin, S., Krzakala, F., Filippone, M., and Daudet, L. Kernel computations from large-scale random features obtained by optical processing units. In *IEEE International Conference on Acoustics, Speech and Signal Processing*, pp. 9294–9298, 2020.

- Park, K. I. *Fundamentals of Probability and Stochastic Processes with Applications to Communications*. Springer, 1st edition, 2018.
- Paszke, A. et al. PyTorch: An Imperative Style, High-Performance Deep Learning Library. In *Advances in Neural Information Processing Systems 32*, pp. 8026–8037. Curran Associates, Inc., 2019.
- Pedregosa, F., , et al. Scikit-learn: Machine learning in Python. *Journal of Machine Learning Research*, 12:2825–2830, 2011.
- Pennington, J., Yu, F. X. X., and Kumar, S. Spherical random features for polynomial kernels. In *Advances in Neural Information Processing Systems 28*, pp. 1846–1854. Curran Associates, Inc., 2015.
- Pham, N. and Pagh, R. Fast and scalable polynomial kernels via explicit feature maps. In *Proceedings of the 19th ACM SIGKDD International Conference on Knowledge Discovery and Data Mining*, pp. 239–247. Association for Computing Machinery, 2013.
- Rahimi, A. and Recht, B. Random features for large-scale kernel machines. In *Advances in Neural Information Processing Systems 20*, pp. 1177–1184. Curran Associates Inc., 2007.
- Rendle, S. Factorization machines. In *Proceedings of the 2010 IEEE International Conference on Data Mining*, pp. 995–1000, 2010.
- Rudi, A., Carratino, L., and Rosasco, L. Falkon: An optimal large scale kernel method. In *Advances in Neural Information Processing Systems*, volume 30. Curran Associates, Inc., 2017.
- Russakovsky, O. et al. ImageNet Large Scale Visual Recognition Challenge. *International Journal of Computer Vision*, 115(3):211–252, 2015.
- Scholkopf, B. and Smola, A. J. *Learning with Kernels: Support Vector Machines, Regularization, Optimization, and Beyond*. MIT Press, 2002.
- Song, Z., Woodruff, D., Yu, Z., and Zhang, L. Fast sketching of polynomial kernels of polynomial degree. In *Proceedings of the 38th International Conference on Machine Learning*, volume 139 of *Proceedings of Machine Learning Research*, pp. 9812–9823. PMLR, 2021.
- Sutherland, D. J. and Schneider, J. On the error of random fourier features. In *Proceedings of the Thirty-First Conference on Uncertainty in Artificial Intelligence*, pp. 862–871. AUAI Press, 2015.
- Szegedy, C., Vanhoucke, V., Ioffe, S., Shlens, J., and Wojna, Z. Rethinking the inception architecture for computer vision. In *2016 IEEE Conference on Computer Vision and Pattern Recognition*, pp. 2818–2826, 2016.
- Tropp, J. A. Improved analysis of the subsampled randomized hadamard transform. *Advances in Adaptive Data Analysis*, 3(1-2):115–126, 2011.
- Wacker, J., Kanagawa, M., and Filippone, M. Improved random features for dot product kernels. *arXiv preprint arXiv:2201.08712*, 2022.
- Williams, C. K. and Seeger, M. Using the Nyström method to speed up kernel machines. In *Advances in Neural Information Processing Systems 13*, pp. 682–688. Curran Associates, Inc., 2000.
- Woodruff, D. P. Sketching as a tool for numerical linear algebra. *Foundations and Trends in Theoretical Computer Science*, 10(1-2):1–157, 2014.

A. Variance of Complex-to-Real Polynomial Sketches

A.1. The structure of CtR variances

In this section, we derive the general variance structure of CtR-sketches that we will frequently refer to later on. For a complex random variable $z = a + ib$ with $a, b \in \mathbb{R}$, we have $|z|^2 = a^2 + b^2$ and $\text{Re}\{z^2\} = a^2 - b^2$. Combining both equations gives $a^2 = \frac{1}{2}(|z|^2 + \text{Re}\{z^2\})$. The scalar a is real-valued and its variance $\mathbb{V}[a] = \mathbb{E}[a^2] - \mathbb{E}[a]^2$ is thus

$$\mathbb{V}[a] = \frac{1}{2}\text{Re}\{\mathbb{E}[|z|^2] + \mathbb{E}[z^2] - 2\mathbb{E}[a]^2\}. \quad (7)$$

Let $\Phi_C : \mathbb{R}^d \rightarrow \mathbb{C}^D$ be a complex polynomial sketch as defined in Eq. (3) and be $\hat{k}_C(\mathbf{x}, \mathbf{y}) = \Phi_C(\mathbf{x})^\top \overline{\Phi_C(\mathbf{y})} \in \mathbb{C}$ the associated approximate kernel for some $\mathbf{x}, \mathbf{y} \in \mathbb{R}^d$. As the kernel estimate is an unbiased estimate of the real-valued target kernel $k(\mathbf{x}, \mathbf{y})$, we have

$$\mathbb{E}[\hat{k}_C(\mathbf{x}, \mathbf{y})] = \mathbb{E}[\text{Re}\{\hat{k}_C(\mathbf{x}, \mathbf{y})\}] + i \cdot \mathbb{E}[\text{Im}\{\hat{k}_C(\mathbf{x}, \mathbf{y})\}] = k(\mathbf{x}, \mathbf{y}).$$

From this it follows that $\mathbb{E}[\text{Im}\{\hat{k}_C(\mathbf{x}, \mathbf{y})\}] = 0$ and therefore $\mathbb{E}[\hat{k}_C(\mathbf{x}, \mathbf{y})] = \mathbb{E}[\text{Re}\{\hat{k}_C(\mathbf{x}, \mathbf{y})\}] = k(\mathbf{x}, \mathbf{y})$. Setting $z = \hat{k}_C(\mathbf{x}, \mathbf{y})$ and $a = \text{Re}\{\hat{k}_C(\mathbf{x}, \mathbf{y})\} =: \hat{k}_{\text{CtR}}(\mathbf{x}, \mathbf{y})$ in Eq. (7) yields

$$\begin{aligned} \mathbb{V}[\hat{k}_{\text{CtR}}(\mathbf{x}, \mathbf{y})] &= \frac{1}{2}\text{Re}\{\mathbb{E}[|\hat{k}_C(\mathbf{x}, \mathbf{y})|^2] + \mathbb{E}[\hat{k}_C(\mathbf{x}, \mathbf{y})^2] - 2\mathbb{E}[\text{Re}\{\hat{k}_C(\mathbf{x}, \mathbf{y})\}]^2\} \\ &= \frac{1}{2}\text{Re}\{\mathbb{E}[|\hat{k}_C(\mathbf{x}, \mathbf{y})|^2] + \mathbb{E}[\hat{k}_C(\mathbf{x}, \mathbf{y})^2] - 2\mathbb{E}[\hat{k}_C(\mathbf{x}, \mathbf{y})]^2\} \\ &= \frac{1}{2}\text{Re}\{\mathbb{V}[\hat{k}_C(\mathbf{x}, \mathbf{y})] + \mathbb{P}\mathbb{V}[\hat{k}_C(\mathbf{x}, \mathbf{y})]\}, \end{aligned}$$

where $\mathbb{P}\mathbb{V}[\hat{k}_C(\mathbf{x}, \mathbf{y})] := \mathbb{E}[\hat{k}_C(\mathbf{x}, \mathbf{y})^2] - \mathbb{E}[\hat{k}_C(\mathbf{x}, \mathbf{y})]^2 \in \mathbb{C}$ is called the *pseudo-variance* of $\hat{k}_C(\mathbf{x}, \mathbf{y})$ (Park, 2018, Chapter 5). In fact, we show next that $\text{Im}\{\mathbb{P}\mathbb{V}[\hat{k}_C(\mathbf{x}, \mathbf{y})]\} = 0$ for all the polynomial sketches discussed in this work. Hence, we can also write $\mathbb{V}[\hat{k}_{\text{CtR}}(\mathbf{x}, \mathbf{y})] = \frac{1}{2}(\mathbb{V}[\hat{k}_C(\mathbf{x}, \mathbf{y})] + \mathbb{P}\mathbb{V}[\hat{k}_C(\mathbf{x}, \mathbf{y})])$ for them since $\mathbb{V}[z] \in \mathbb{R}$ for any $z \in \mathbb{C}$. In order to determine $\mathbb{V}[\hat{k}_{\text{CtR}}(\mathbf{x}, \mathbf{y})]$, we thus work out $\mathbb{V}[\hat{k}_C(\mathbf{x}, \mathbf{y})]$ and $\mathbb{P}\mathbb{V}[\hat{k}_C(\mathbf{x}, \mathbf{y})]$ for Gaussian, Rademacher and TensorSRHT sketches in the following.

A.2. Gaussian and Rademacher Polynomial Sketches

In this section, we work out the variance of Gaussian and Rademacher CtR-sketches. For a set of D i.i.d. random feature samples, we have

$$\mathbb{V}[\hat{k}_{\text{CtR}}(\mathbf{x}, \mathbf{y})] = \mathbb{V}[\text{Re}\{\hat{k}_C(\mathbf{x}, \mathbf{y})\}] = \mathbb{V}\left[\text{Re}\left\{\Phi_C(\mathbf{x})^\top \overline{\Phi_C(\mathbf{y})}\right\}\right] = \frac{1}{D^2} \sum_{\ell=1}^D \mathbb{V}\left[\text{Re}\left\{\prod_{i=1}^p (\mathbf{w}_{i,\ell}^\top \mathbf{x})(\overline{\mathbf{w}_{i,\ell}^\top \mathbf{y}})\right\}\right]. \quad (8)$$

As $\{\mathbf{w}_{i,\ell}\}_{\ell=1}^D$ are i.i.d., the variance terms are equal for each ℓ in Eq. (8) and $\mathbb{V}[\hat{k}_{\text{CtR}}(\mathbf{x}, \mathbf{y})] \propto 1/D$. We can therefore assume $D = 1$ and drop the index ℓ for simplicity in the following. We then rescale the variances by $1/D$ later.

As our estimator is unbiased, we have $\mathbb{E}[\hat{k}_C(\mathbf{x}, \mathbf{y})] = k(\mathbf{x}, \mathbf{y}) = (\mathbf{x}^\top \mathbf{y})^p$. Thus, we only need to work out $\mathbb{E}[|\hat{k}_C(\mathbf{x}, \mathbf{y})|^2]$ and $\mathbb{E}[\hat{k}_C(\mathbf{x}, \mathbf{y})^2]$ for the variance and pseudo-variance, respectively.

Pseudo-Variance. We start with $\mathbb{E}[\hat{k}_C(\mathbf{x}, \mathbf{y})^2]$ to derive the pseudo-variance $\mathbb{P}\mathbb{V}[\hat{k}_C(\mathbf{x}, \mathbf{y})]$ after.

$$\mathbb{E}[\hat{k}_C(\mathbf{x}, \mathbf{y})^2] = \mathbb{E}\left[\left(\prod_{i=1}^p \mathbf{w}_i^\top \mathbf{x} \overline{\mathbf{w}_i^\top \mathbf{y}}\right)^2\right] = \prod_{i=1}^p \mathbb{E}\left[(\mathbf{w}_i^\top \mathbf{x})^2 (\overline{\mathbf{w}_i^\top \mathbf{y}})^2\right] = \mathbb{E}\left[(\mathbf{w}^\top \mathbf{x})^2 (\overline{\mathbf{w}^\top \mathbf{y}})^2\right]^p \quad (9)$$

$$= \left(\sum_{i=1}^d \sum_{j=1}^d \sum_{k=1}^d \sum_{l=1}^d \mathbb{E}[w_i w_j \overline{w_k w_l}] x_i x_j y_k y_l\right)^p \quad (10)$$

$\mathbb{E}_{ij\overline{kl}} := \mathbb{E}[w_i w_j \overline{w_k w_l}] \neq 0$, only if:

1. $i = j = k = l$: there are d terms $(\mathbb{E}_{i\bar{j}\bar{k}l})x_i x_j y_k y_l = \mathbb{E}[|w_i|^4]x_i^2 y_i^2$.
2. $i = k \neq j = l$: there are $d(d-1)$ terms $(\mathbb{E}_{i\bar{j}\bar{k}l})x_i x_j y_k y_l = \mathbb{E}[|w_i|^2]x_i y_i \mathbb{E}[|w_j|^2]x_j y_j = x_i y_i x_j y_j$.
3. $i = l \neq j = k$: there are $d(d-1)$ terms $(\mathbb{E}_{i\bar{j}\bar{k}l})x_i x_j y_k y_l = \mathbb{E}[|w_i|^2]x_i y_i \mathbb{E}[|w_j|^2]x_j y_j = x_i y_i x_j y_j$.

As for both the Gaussian and the Rademacher sketch, we have $\mathbb{E}[|w_i|^2] = 1$ for all $\{w_i\}_{i=1}^d$, we obtain:

$$\mathbb{E}[\hat{k}_C(\mathbf{x}, \mathbf{y})^2] = \left(\sum_{i=1}^d \mathbb{E}[|w_i|^4]x_i^2 y_i^2 + 2 \sum_{i=1}^d \sum_{j \neq i}^d x_i y_i x_j y_j \right)^p \quad (11)$$

We have $\mathbb{E}[|w_i|^4] = 2$ and $\mathbb{E}[|w_i|^4] = 1$ for the Gaussian and Rademacher case, respectively. So the pseudo-variances $\mathbb{V}[\hat{k}_C(\mathbf{x}, \mathbf{y})] = \mathbb{E}[\hat{k}_C(\mathbf{x}, \mathbf{y})^2] - \mathbb{E}[\hat{k}_C(\mathbf{x}, \mathbf{y})]^2$ are given by the following real-valued expressions:

$$\mathbb{P}\mathbb{V}[\hat{k}_C(\mathbf{x}, \mathbf{y})] = \frac{1}{D} \left((2(\mathbf{x}^\top \mathbf{y})^2)^p - (\mathbf{x}^\top \mathbf{y})^{2p} \right) \quad (\text{Gaussian}) \quad (12)$$

$$\mathbb{P}\mathbb{V}[\hat{k}_C(\mathbf{x}, \mathbf{y})] = \frac{1}{D} \left(\left(2(\mathbf{x}^\top \mathbf{y})^2 - \sum_{i=1}^d x_i^2 y_i^2 \right)^p - (\mathbf{x}^\top \mathbf{y})^{2p} \right) \quad (\text{Rademacher}) \quad (13)$$

where we added the $1/D$ scaling that we left out before. Note that $\mathbb{E}[|w_i|^4] \geq (\mathbb{E}[|w_i|^2])^2 = 1$ by Jensen's inequality, which is why the Rademacher sketch yields the lowest possible pseudo-variance for the estimator studied in Section 3.1.

Variance. We work out $\mathbb{E}[|\hat{k}_C(\mathbf{x}, \mathbf{y})|^2]$ to derive the variance $\mathbb{V}[\hat{k}_C(\mathbf{x}, \mathbf{y})]$.

$$\begin{aligned} \mathbb{E}[|\hat{k}_C(\mathbf{x}, \mathbf{y})|^2] &= \mathbb{E} \left[\left| \prod_{i=1}^p \mathbf{w}_i^\top \mathbf{x} \overline{\mathbf{w}_i^\top \mathbf{y}} \right|^2 \right] = \mathbb{E} \left[\prod_{i=1}^p |\mathbf{w}_i^\top \mathbf{x}|^2 |\overline{\mathbf{w}_i^\top \mathbf{y}}|^2 \right] \\ &= \mathbb{E} \left[\left(\sum_{i=1}^d w_i x_i \right) \left(\sum_{j=1}^d \overline{w_j} y_j \right) \left(\sum_{k=1}^d \overline{w_k} x_k \right) \left(\sum_{l=1}^d w_l y_l \right) \right]^p = \left(\sum_{i=1}^d \sum_{j=1}^d \sum_{k=1}^d \sum_{l=1}^d \mathbb{E}[w_i \overline{w_j} \overline{w_k} w_l] x_i y_j x_k y_l \right)^p. \end{aligned} \quad (14)$$

Now we check when $\mathbb{E}_{i\bar{j}\bar{k}l} := \mathbb{E}[w_i \overline{w_j} \overline{w_k} w_l] \neq 0$ holds. The analysis is the same as before with differently placed conjugates leading to different expressions.

1. $i = j = k = l$: there are d terms $(\mathbb{E}_{i\bar{j}\bar{k}l})x_i y_j x_k y_l = \mathbb{E}[|w_i|^4]x_i^2 y_i^2$.
2. $i = j \neq k = l$: there are $d(d-1)$ terms $(\mathbb{E}_{i\bar{j}\bar{k}l})x_i y_j x_k y_l = \mathbb{E}[|w_i|^2] \mathbb{E}[|w_k|^2] x_i x_k y_i y_k$.
3. $i = k \neq j = l$, there are $d(d-1)$ terms $(\mathbb{E}_{i\bar{j}\bar{k}l})x_i y_j x_k y_l = \mathbb{E}[|w_i|^2] \mathbb{E}[|w_j|^2] x_i^2 y_j^2$.
4. $i = l \neq j = k$, there are $d(d-1)$ terms $(\mathbb{E}_{i\bar{j}\bar{k}l})x_i y_j x_k y_l = \mathbb{E}[w_i^2] \mathbb{E}[\overline{w_j}^2] x_i x_j y_i y_j$.

Therefore,

$$\begin{aligned} \mathbb{E}[|\hat{k}_C(\mathbf{x}, \mathbf{y})|^2] &= \sum_{i=1}^d \mathbb{E}[|w_i|^4]x_i^2 y_i^2 + \sum_{i=1}^d \sum_{\substack{j=1 \\ j \neq i}}^d x_i^2 y_j^2 + \sum_{i=1}^d \sum_{\substack{j=1 \\ j \neq i}}^d x_i x_j y_i y_j + \sum_{i=1}^d \sum_{\substack{j=1 \\ j \neq i}}^d \mathbb{E}[w_i^2] \mathbb{E}[\overline{w_j}^2] x_i x_j y_i y_j \\ &= \sum_{i=1}^d \mathbb{E}[|w_i|^4]x_i^2 y_i^2 + \left[\|\mathbf{x}\|^2 \|\mathbf{y}\|^2 - \sum_{i=1}^d x_i^2 y_i^2 \right] + \left[(\mathbf{x}^\top \mathbf{y})^2 - \sum_{i=1}^d x_i^2 y_i^2 \right] + \sum_{i=1}^d \sum_{\substack{j=1 \\ j \neq i}}^d \mathbb{E}[w_i^2] \mathbb{E}[\overline{w_j}^2] x_i x_j y_i y_j \end{aligned}$$

Once again, we have $\mathbb{E}[|w_i|^4] = 2$ and $\mathbb{E}[|w_i|^4] = 1$ for the Gaussian and Rademacher case, respectively. For complex-valued polynomial sketches, we have $\mathbb{E}[w_i^2] = 0$ because $\text{Re}\{w_i^2\}$ and $\text{Im}\{w_i^2\}$ are independent with zero mean. For

real-valued polynomial sketches on the other hand, we have $\mathbb{E}[w_i^2] = \mathbb{E}[\overline{w_i^2}] = 1$. Let $q = 2$ for the real and $q = 1$ for the complex case, respectively. We obtain the following variances $\mathbb{V}[\hat{k}_C(\mathbf{x}, \mathbf{y})] = \mathbb{E}[|\hat{k}_C(\mathbf{x}, \mathbf{y})|^2] - |\mathbb{E}[\hat{k}_C(\mathbf{x}, \mathbf{y})]|^2$:

$$\mathbb{V}[\hat{k}_C(\mathbf{x}, \mathbf{y})] = \frac{1}{D} \left(\left(\|\mathbf{x}\|^2 \|\mathbf{y}\|^2 + q(\mathbf{x}^\top \mathbf{y})^2 \right)^p - (\mathbf{x}^\top \mathbf{y})^{2p} \right) \quad (\text{Gaussian}) \quad (15)$$

$$\mathbb{V}[\hat{k}_C(\mathbf{x}, \mathbf{y})] = \frac{1}{D} \left(\left(\|\mathbf{x}\|^2 \|\mathbf{y}\|^2 + q \sum_{i=1}^d \sum_{j \neq i}^d x_i x_j y_i y_j \right)^p - (\mathbf{x}^\top \mathbf{y})^{2p} \right) \quad (\text{Rademacher}) \quad (16)$$

where we added the $1/D$ scaling that we left out before. Note that $\mathbb{E}[|w_i|^4] \geq (\mathbb{E}[|w_i|^2])^2 = 1$ by Jensen's inequality, which is why the Rademacher sketch yields the lowest possible variance for the estimator studied in Section 3.1. As both the variance as well as the pseudo-variance lower bound are attained, the Rademacher sketch also has the lowest CtR-variance through Eq. (6).

A.3. Gaussian and Rademacher CtR variance advantage over their real-valued analogs

In the following, we compare Gaussian and Rademacher CtR-sketches against their real-valued analogs assuming that the corresponding feature maps have equal dimensions. Thus, we assign $2D$ random features to the real feature map $\Phi_R : \mathbb{R}^d \rightarrow \mathbb{R}^{2D}$ and only D random features to the CtR feature map $\Phi_{\text{CtR}} : \mathbb{R}^d \rightarrow \mathbb{R}^{2D}$ as it has twice as many dimensions for the same number of features.

We call the corresponding kernel estimates $\hat{k}_R(\mathbf{x}, \mathbf{y}) = \Phi_R(\mathbf{x})^\top \Phi_R(\mathbf{y})$ and $\hat{k}_{\text{CtR}}(\mathbf{x}, \mathbf{y}) = \Phi_{\text{CtR}}(\mathbf{x})^\top \Phi_{\text{CtR}}(\mathbf{y})$. $\mathbb{V}[\hat{k}_R(\mathbf{x}, \mathbf{y})]$ is given in Eq. (15) and (16), where we set $q = 2$.

We further have $\mathbb{V}[\hat{k}_{\text{CtR}}(\mathbf{x}, \mathbf{y})] = \frac{1}{2}(\mathbb{V}[\hat{k}_C(\mathbf{x}, \mathbf{y})] + \mathbb{P}\mathbb{V}[\hat{k}_C(\mathbf{x}, \mathbf{y})])$ as shown in Section A.1. $\mathbb{V}[\hat{k}_C(\mathbf{x}, \mathbf{y})]$ is given in Eq. (15) and (16), where we set $q = 1$. $\mathbb{P}\mathbb{V}[\hat{k}_C(\mathbf{x}, \mathbf{y})]$ is given in Eq. (12) and (13), respectively.

We start with the simpler Gaussian case and study the Rademacher case after.

A.3.1. GAUSSIAN CASE: PROOF OF THEOREM (4.2).

Proof Taking into account the different number of random features for Φ_R and Φ_{CtR} to have equal dimensions, the variance difference of their kernel estimates yields:

$$\begin{aligned} & \mathbb{V}[\hat{k}_R(\mathbf{x}, \mathbf{y})] - \mathbb{V}[\hat{k}_{\text{CtR}}(\mathbf{x}, \mathbf{y})] \\ &= \frac{1}{2D} \left(\left(\|\mathbf{x}\|^2 \|\mathbf{y}\|^2 + 2(\mathbf{x}^\top \mathbf{y})^2 \right)^p - (\mathbf{x}^\top \mathbf{y})^{2p} \right) - \frac{1}{2D} \left(\left(\|\mathbf{x}\|^2 \|\mathbf{y}\|^2 + (\mathbf{x}^\top \mathbf{y})^2 \right)^p + (2(\mathbf{x}^\top \mathbf{y})^2)^p - 2(\mathbf{x}^\top \mathbf{y})^{2p} \right) \\ &= \frac{1}{2D} \left(\left(\|\mathbf{x}\|^2 \|\mathbf{y}\|^2 + 2(\mathbf{x}^\top \mathbf{y})^2 \right)^p - (2(\mathbf{x}^\top \mathbf{y})^2)^p \right) - \frac{1}{2D} \left(\left(\|\mathbf{x}\|^2 \|\mathbf{y}\|^2 + (\mathbf{x}^\top \mathbf{y})^2 \right)^p - (\mathbf{x}^\top \mathbf{y})^{2p} \right) \\ &= \frac{1}{2D} \sum_{k=0}^{p-1} \binom{p}{k} (2(\mathbf{x}^\top \mathbf{y})^2)^k \left(\|\mathbf{x}\|^2 \|\mathbf{y}\|^2 \right)^{p-k} - \frac{1}{2D} \sum_{k=0}^{p-1} \binom{p}{k} (\mathbf{x}^\top \mathbf{y})^{2k} \left(\|\mathbf{x}\|^2 \|\mathbf{y}\|^2 \right)^{p-k} \\ &= \frac{1}{2D} \sum_{k=0}^{p-1} \binom{p}{k} (2^k - 1) (\mathbf{x}^\top \mathbf{y})^{2k} \left(\|\mathbf{x}\|^2 \|\mathbf{y}\|^2 \right)^{p-k} \geq 0 \end{aligned}$$

■

Thus, the Gaussian CtR-estimator is always better regardless of the choice of \mathbf{x} , \mathbf{y} and p and despite using only half the random feature samples. Note that the variance difference is zero if $p = 1$ and increases as p increases. Moreover, the difference is maximized for parallel \mathbf{x} and \mathbf{y} . In this case, we have $(\mathbf{x}^\top \mathbf{y}) = \|\mathbf{x}\| \|\mathbf{y}\|$ and the difference becomes

$$\mathbb{V}[\hat{k}_R(\mathbf{x}, \mathbf{y})] - \mathbb{V}[\hat{k}_{\text{CtR}}(\mathbf{x}, \mathbf{y})] = \frac{1}{2D} \sum_{k=0}^{p-1} \binom{p}{k} (2^k - 1) \left(\|\mathbf{x}\|^2 \|\mathbf{y}\|^2 \right)^p = \frac{1}{2D} \|\mathbf{x}\|^{2p} \|\mathbf{y}\|^{2p} (3^p - 2^{p+1} + 1)$$

We analyze the more difficult Rademacher case next.

A.3.2. RADEMACHER CASE: PROOF OF THEOREM (4.1).

Proof Taking into account the different number of random features for Φ_R and Φ_{CtR} to have equal dimensions, the variance difference of their kernel estimates yields:

$$\begin{aligned} & \mathbb{V}[\hat{k}_R(\mathbf{x}, \mathbf{y})] - \mathbb{V}[\hat{k}_{\text{CtR}}(\mathbf{x}, \mathbf{y})] \\ &= \frac{1}{2D} \left(\left(\|\mathbf{x}\|^2 \|\mathbf{y}\|^2 + 2 \sum_{i=1}^d \sum_{j \neq i} x_i x_j y_i y_j \right)^p - (\mathbf{x}^\top \mathbf{y})^{2p} \right) \\ & \quad - \frac{1}{2D} \left\{ \left(\|\mathbf{x}\|^2 \|\mathbf{y}\|^2 + \sum_{i=1}^d \sum_{j \neq i} x_i x_j y_i y_j \right)^p - (\mathbf{x}^\top \mathbf{y})^{2p} + \left(2(\mathbf{x}^\top \mathbf{y})^2 - \sum_{i=1}^d x_i^2 y_i^2 \right)^p - (\mathbf{x}^\top \mathbf{y})^{2p} \right\} \end{aligned}$$

Next, we write $(\mathbf{x}^\top \mathbf{y})^{2p} = ((\mathbf{x}^\top \mathbf{y})^2 - \sum_{i=1}^d x_i^2 y_i^2 + \sum_{i=1}^d x_i^2 y_i^2)^p$. In this way, we can factor out the term $a := (\mathbf{x}^\top \mathbf{y})^2 - \sum_{i=1}^d x_i^2 y_i^2 = \sum_{i=1}^d \sum_{j \neq i} x_i x_j y_i y_j$ and apply the binomial theorem to *all* addends. This gives:

$$\begin{aligned} \mathbb{V}[\hat{k}_R(\mathbf{x}, \mathbf{y})] - \mathbb{V}[\hat{k}_{\text{CtR}}(\mathbf{x}, \mathbf{y})] &= \frac{1}{2D} \sum_{k=0}^p \binom{p}{k} a^{p-k} \\ & \quad \left(\left(\|\mathbf{x}\|^2 \|\mathbf{y}\|^2 + (\mathbf{x}^\top \mathbf{y})^2 - \sum_{i=1}^d x_i^2 y_i^2 \right)^k - \left((\|\mathbf{x}\|^2 \|\mathbf{y}\|^2)^k + (\mathbf{x}^\top \mathbf{y})^{2k} - \left(\sum_{i=1}^d x_i^2 y_i^2 \right)^k \right) \right) \end{aligned}$$

We now show that the following term is always non-negative:

$$B := \left(\left(\|\mathbf{x}\|^2 \|\mathbf{y}\|^2 + (\mathbf{x}^\top \mathbf{y})^2 - \sum_{i=1}^d x_i^2 y_i^2 \right)^k - \left((\|\mathbf{x}\|^2 \|\mathbf{y}\|^2)^k + (\mathbf{x}^\top \mathbf{y})^{2k} - \left(\sum_{i=1}^d x_i^2 y_i^2 \right)^k \right) \right) \quad (17)$$

For $k = 0$ and $k = 1$, $B = 0$. For $k \geq 2$, we have:

$$\left(\|\mathbf{x}\|^2 \|\mathbf{y}\|^2 + (\mathbf{x}^\top \mathbf{y})^2 - \sum_{i=1}^d x_i^2 y_i^2 \right)^k = \sum_{j=0}^k \binom{k}{j} \|\mathbf{x}\|^{2j} \|\mathbf{y}\|^{2j} \left((\mathbf{x}^\top \mathbf{y})^2 - \sum_{i=1}^d x_i^2 y_i^2 \right)^{k-j}$$

Plugging this expression into B and cancelling out the addend for $j = k$ yields:

$$B = \sum_{j=0}^{k-1} \binom{k}{j} \|\mathbf{x}\|^{2j} \|\mathbf{y}\|^{2j} \left((\mathbf{x}^\top \mathbf{y})^2 - \sum_{i=1}^d x_i^2 y_i^2 \right)^{k-j} - \left((\mathbf{x}^\top \mathbf{y})^{2k} - \left(\sum_{i=1}^d x_i^2 y_i^2 \right)^k \right)$$

Next, we refactor $(\mathbf{x}^\top \mathbf{y})^{2k} - \left(\sum_{i=1}^d x_i^2 y_i^2 \right)^k$:

$$\begin{aligned} (\mathbf{x}^\top \mathbf{y})^{2k} - \left(\sum_{i=1}^d x_i^2 y_i^2 \right)^k &= \left((\mathbf{x}^\top \mathbf{y})^2 - \sum_{i=1}^d x_i^2 y_i^2 + \sum_{i=1}^d x_i^2 y_i^2 \right)^k - \left(\sum_{i=1}^d x_i^2 y_i^2 \right)^k \\ &= \sum_{j=0}^k \binom{k}{j} \left(\sum_{i=1}^d x_i^2 y_i^2 \right)^j \left((\mathbf{x}^\top \mathbf{y})^2 - \sum_{i=1}^d x_i^2 y_i^2 \right)^{k-j} - \left(\sum_{i=1}^d x_i^2 y_i^2 \right)^k \\ &= \sum_{j=0}^{k-1} \binom{k}{j} \left(\sum_{i=1}^d x_i^2 y_i^2 \right)^j \left((\mathbf{x}^\top \mathbf{y})^2 - \sum_{i=1}^d x_i^2 y_i^2 \right)^{k-j} \end{aligned}$$

Plugging this expression into B yields:

$$B = \sum_{j=0}^{k-1} \binom{k}{j} \left(\|\mathbf{x}\|^{2j} \|\mathbf{y}\|^{2j} - \left(\sum_{i=1}^d x_i^2 y_i^2 \right)^j \right) \left((\mathbf{x}^\top \mathbf{y})^2 - \sum_{i=1}^d x_i^2 y_i^2 \right)^{k-j}$$

Finally, we insert B back into the original variance difference $\mathbb{V}[\hat{k}_R(\mathbf{x}, \mathbf{y})] - \mathbb{V}[\hat{k}_{\text{CTR}}(\mathbf{x}, \mathbf{y})]$ (remember that $B = 0$ if $k < 2$):

$$\mathbb{V}[\hat{k}_R(\mathbf{x}, \mathbf{y})] - \mathbb{V}[\hat{k}_{\text{CTR}}(\mathbf{x}, \mathbf{y})] = \frac{1}{2D} \sum_{k=2}^p \binom{p}{k} a^{p-k} B = \frac{1}{2D} \sum_{k=2}^p \sum_{j=0}^{k-1} \binom{p}{k} \binom{k}{j} a^{p-j} \left(\|\mathbf{x}\|^{2j} \|\mathbf{y}\|^{2j} - \left(\sum_{i=1}^d x_i^2 y_i^2 \right)^j \right)$$

Finally, we note that $b := \|\mathbf{x}\|^{2j} \|\mathbf{y}\|^{2j} - \left(\sum_{i=1}^d x_i^2 y_i^2 \right)^j = \left(\sum_{i=1}^d \sum_{\ell=1}^d x_i^2 y_\ell^2 \right)^j - \left(\sum_{i=1}^d x_i^2 y_i^2 \right)^j \geq 0$ and $\mathbb{V}[\hat{k}_R(\mathbf{x}, \mathbf{y})] - \mathbb{V}[\hat{k}_{\text{CTR}}(\mathbf{x}, \mathbf{y})] \geq 0$ if $a = \sum_{i=1}^d \sum_{j \neq i} x_i x_j y_i y_j^2 \geq 0$. ■

A.3.3. ALTERNATIVE VARIANCE DERIVATION FOR GAUSSIAN POLYNOMIAL SKETCHES WHEN $p = 2$

In this section, we provide an alternative variance derivation for Gaussian CtR-sketches by explicitly expanding the real-valued approximate kernel $\hat{k}_{\text{CTR}}(\mathbf{x}, \mathbf{y})$ (5). This derivation provides us with novel insights about the origin of the variance reduction that we derived in Section A.3.1.

We consider $D = 1$ random feature for ease of presentation. For Gaussian polynomial sketches we have $\mathbf{w}_i \sim \mathcal{CN}(\mathbf{0}, \mathbf{I}_d)$ with $\mathbf{w}_i \in \mathbb{C}^d$ for $i \in \{1, \dots, p\}$ as introduced in Section 3.1 (we dropped the index ℓ here). Let $\mathbf{w}_i = \mathbf{a}_i + i\mathbf{b}_i$ where $\mathbf{a}_i = \text{Re}(\mathbf{w}_i) \sim \mathcal{N}(\mathbf{0}, \frac{1}{2}\mathbf{I}_d)$ and $\mathbf{b}_i = \text{Im}(\mathbf{w}_i) \sim \mathcal{N}(\mathbf{0}, \frac{1}{2}\mathbf{I}_d)$ are independent samples. We look at the specific case $p = 2$ and start by expanding the complex-valued approximate kernel

$$\begin{aligned} \hat{k}_C(\mathbf{x}, \mathbf{y}) &= \Phi_C(\mathbf{x}) \overline{\Phi_C(\mathbf{y})} = \prod_{i=1}^p (\mathbf{a}_i^\top \mathbf{x} + i\mathbf{b}_i^\top \mathbf{x}) \overline{\prod_{i=1}^p (\mathbf{a}_i^\top \mathbf{y} + i\mathbf{b}_i^\top \mathbf{y})} = \prod_{i=1}^p (\mathbf{a}_i^\top \mathbf{x} + i\mathbf{b}_i^\top \mathbf{x}) \prod_{i=1}^p (\mathbf{a}_i^\top \mathbf{y} - i\mathbf{b}_i^\top \mathbf{y}) \\ &= \left(\underbrace{\mathbf{x}^\top \mathbf{a}_1 \mathbf{a}_2^\top \mathbf{x}}_{A^x} - \underbrace{\mathbf{x}^\top \mathbf{b}_1 \mathbf{b}_2^\top \mathbf{x}}_{B^x} + i \left(\underbrace{\mathbf{x}^\top \mathbf{b}_1 \mathbf{a}_2^\top \mathbf{x}}_{C^x} + \underbrace{\mathbf{x}^\top \mathbf{b}_2 \mathbf{a}_1^\top \mathbf{x}}_{D^x} \right) \right) \cdot \left(\underbrace{\mathbf{y}^\top \mathbf{a}_1 \mathbf{a}_2^\top \mathbf{y}}_{A^y} - \underbrace{\mathbf{y}^\top \mathbf{b}_1 \mathbf{b}_2^\top \mathbf{y}}_{B^y} - i \left(\underbrace{\mathbf{y}^\top \mathbf{b}_1 \mathbf{a}_2^\top \mathbf{y}}_{C^y} + \underbrace{\mathbf{y}^\top \mathbf{b}_2 \mathbf{a}_1^\top \mathbf{y}}_{D^y} \right) \right) \\ &= A^x A^y - A^x B^y - B^x A^y + B^x B^y + C^x C^y + C^x D^y + D^x C^y + D^x D^y \\ &\quad + i (B^x C^y + B^x D^y - A^x C^y - A^x D^y + C^x A^y - C^x B^y + D^x A^y - D^x B^y) \end{aligned}$$

The Gaussian CtR kernel estimate $\hat{k}_{\text{CTR}}(\mathbf{x}, \mathbf{y})$ (5) is then obtained by taking the real part of the above expression:

$$\hat{k}_{\text{CTR}}(\mathbf{x}, \mathbf{y}) = \text{Re}\{\hat{k}_C(\mathbf{x}, \mathbf{y})\} = A^x A^y - A^x B^y - B^x A^y + B^x B^y + C^x C^y + C^x D^y + D^x C^y + D^x D^y$$

In the following, we rederive the variance of this estimator. Recall that we derived the variance for arbitrary p in Section A.2 already. Here we apply the formula $\mathbb{V}[\sum_{i=1}^n X_i] = \sum_{i=1}^n \mathbb{V}[X_i] + 2 \sum_{i=1}^n \sum_{j \neq i} \text{Cov}(X_i, X_j)$.

$$\begin{aligned} \mathbb{V}[\hat{k}_{\text{CTR}}(\mathbf{x}, \mathbf{y})] &= \mathbb{V}[A^x A^y - A^x B^y - B^x A^y + B^x B^y + C^x C^y + C^x D^y + D^x C^y + D^x D^y] \\ &= \mathbb{V}[A^x A^y] + \mathbb{V}[A^x B^y] + \mathbb{V}[B^x A^y] + \mathbb{V}[B^x B^y] + \mathbb{V}[C^x C^y] + \mathbb{V}[C^x D^y] + \mathbb{V}[D^x C^y] + \mathbb{V}[D^x D^y] \\ &\quad + 2 \left[-\text{Cov}(A^x A^y, A^x B^y) - \text{Cov}(A^x A^y, B^x A^y) + \text{Cov}(A^x A^y, B^x B^y) + \text{Cov}(A^x A^y, C^x C^y) \right. \\ &\quad + \text{Cov}(A^x A^y, C^x D^y) + \text{Cov}(A^x A^y, D^x C^y) + \text{Cov}(A^x A^y, D^x D^y) + \text{Cov}(A^x B^y, B^x A^y) \\ &\quad - \text{Cov}(A^x B^y, B^x B^y) - \text{Cov}(A^x B^y, C^x C^y) - \text{Cov}(A^x B^y, C^x D^y) - \text{Cov}(A^x B^y, D^x C^y) \\ &\quad - \text{Cov}(A^x B^y, D^x D^y) - \text{Cov}(B^x A^y, B^x B^y) - \text{Cov}(B^x A^y, C^x C^y) - \text{Cov}(B^x A^y, C^x D^y) \\ &\quad - \text{Cov}(B^x A^y, D^x C^y) - \text{Cov}(B^x A^y, D^x D^y) + \text{Cov}(B^x B^y, C^x C^y) + \text{Cov}(B^x B^y, C^x D^y) \\ &\quad + \text{Cov}(B^x B^y, D^x C^y) + \text{Cov}(B^x B^y, D^x D^y) + \text{Cov}(C^x C^y, C^x D^y) + \text{Cov}(C^x C^y, D^x C^y) \\ &\quad \left. + \text{Cov}(C^x C^y, D^x D^y) + \text{Cov}(C^x D^y, D^x C^y) + \text{Cov}(C^x D^y, D^x D^y) + \text{Cov}(D^x C^y, D^x D^y) \right] \end{aligned}$$

18 out of the 28 covariance terms are equal to zero. We compute and summarize the rest of the terms:

$$\begin{aligned}\mathbb{V}[A^x A^y] &= \mathbb{V}[B^x B^y] = \mathbb{V}[C^x C^y] = \mathbb{V}[D^x D^y] = \frac{1}{16}(\|\mathbf{x}\|^2 \|\mathbf{y}\|^2 + 2(\mathbf{x}^\top \mathbf{y})^2) - \frac{1}{16}(\mathbf{x}^\top \mathbf{y})^4 \\ \mathbb{V}[A^x B^y] &= \mathbb{V}[B^x A^y] = \mathbb{V}[C^x D^y] = \mathbb{V}[D^x C^y] = \frac{1}{16} \|\mathbf{x}\|^4 \|\mathbf{y}\|^4 \\ \text{Cov}(A^x A^y, C^x C^y) &= \text{Cov}(A^x A^y, D^x D^y) = \text{Cov}(B^x B^y, C^x C^y) = \text{Cov}(B^x B^y, D^x D^y) = \frac{1}{16}((\mathbf{x}^\top \mathbf{y})^2 \|\mathbf{x}\|^2 \|\mathbf{y}\|^2 + (\mathbf{x}^\top \mathbf{y})^4) \\ \text{Cov}(A^x B^y, B^x A^y) &= \text{Cov}(C^x D^y, D^x C^y) = \frac{1}{16}(\mathbf{x}^\top \mathbf{y})^4 \\ \text{Cov}(A^x B^y, C^x D^y) &= \text{Cov}(A^x B^y, D^x C^y) = \text{Cov}(B^x A^y, C^x D^y) = \text{Cov}(B^x A^y, D^x C^y) = \frac{1}{16} \|\mathbf{x}\|^2 \|\mathbf{y}\|^2 (\mathbf{x}^\top \mathbf{y})^2\end{aligned}$$

We complete the variance derivation by grouping up equal terms:

$$\begin{aligned}\mathbb{V}[\hat{k}_{\text{CtR}}(\mathbf{x}, \mathbf{y})] &= 4 \mathbb{V}[A^x A^y] + 4 \mathbb{V}[A^x B^y] + 2(4 \text{Cov}(A^x A^y, C^x C^y) + 2 \text{Cov}(A^x B^y, B^x A^y) - 4 \text{Cov}(A^x B^y, C^x D^y)) \\ &= 4 \mathbb{V}[A^x A^y] + 4 \mathbb{V}[A^x B^y] + 2 \times \frac{6}{16}(\mathbf{x}^\top \mathbf{y})^4 \\ &= 4 \mathbb{V}[A^x A^y] + \frac{4}{16} \|\mathbf{x}\|^4 \|\mathbf{y}\|^4 + 2 \times \frac{6}{16}(\mathbf{x}^\top \mathbf{y})^4 \tag{18} \\ &= \frac{4}{16}((\|\mathbf{x}\|^2 \|\mathbf{y}\|^2 + 2(\mathbf{x}^\top \mathbf{y})^2)^2 - (\mathbf{x}^\top \mathbf{y})^4) + \frac{4}{16} \|\mathbf{x}\|^4 \|\mathbf{y}\|^4 + 2 \times \frac{6}{16}(\mathbf{x}^\top \mathbf{y})^4 \\ &= \frac{4}{16}((\|\mathbf{x}\|^4 \|\mathbf{y}\|^4 + 4 \|\mathbf{x}\|^2 \|\mathbf{y}\|^2 (\mathbf{x}^\top \mathbf{y})^2 + 3(\mathbf{x}^\top \mathbf{y})^4)) + \frac{4}{16} \|\mathbf{x}\|^4 \|\mathbf{y}\|^4 + 2 \times \frac{6}{16}(\mathbf{x}^\top \mathbf{y})^4 \\ &= \frac{1}{2} \|\mathbf{x}\|^4 \|\mathbf{y}\|^4 + \|\mathbf{x}\|^2 \|\mathbf{y}\|^2 (\mathbf{x}^\top \mathbf{y})^2 + \frac{3}{2}(\mathbf{x}^\top \mathbf{y})^4 \\ &= \frac{1}{2} \underbrace{((\|\mathbf{x}\|^2 \|\mathbf{y}\|^2 + (\mathbf{x}^\top \mathbf{y})^2)^2 - (\mathbf{x}^\top \mathbf{y})^4)}_{\mathbb{V}[\hat{k}_{\text{C}}(\mathbf{x}, \mathbf{y})]} + \frac{1}{2} \underbrace{((2(\mathbf{x}^\top \mathbf{y})^2)^2 - (\mathbf{x}^\top \mathbf{y})^4)}_{\mathbb{P}\mathbb{V}[\hat{k}_{\text{C}}(\mathbf{x}, \mathbf{y})]}\end{aligned}$$

We thus recover the CtR-variance (6) of Gaussian polynomial sketches with $p = 2$, where $\mathbb{V}[\hat{k}_{\text{C}}(\mathbf{x}, \mathbf{y})]$ is the variance (15) and $\mathbb{P}\mathbb{V}[\hat{k}_{\text{C}}(\mathbf{x}, \mathbf{y})]$ is the pseudo-variance (12) of the complex Gaussian polynomial sketch.

A.3.4. ANALYZING THE VARIANCE REDUCTION OVER REAL GAUSSIAN SKETCHES

We study the variance reduction of the CtR-Gaussian sketch over its real analog. For this purpose, we take a closer look at Eq. (18) that summarizes the variance as:

$$\mathbb{V}[\hat{k}_{\text{CtR}}(\mathbf{x}, \mathbf{y})] = \underbrace{4 \mathbb{V}[A^x A^y]}_{\text{(A)}} + \underbrace{4 \mathbb{V}[A^x B^y]}_{\text{(B)}} + \underbrace{2 \times \frac{6}{16}(\mathbf{x}^\top \mathbf{y})^4}_{\text{(C)}}$$

(A) is the contribution of the variances $\mathbb{V}[A^x A^y], \mathbb{V}[B^x B^y], \mathbb{V}[C^x C^y], \mathbb{V}[D^x D^y]$. It is a downscaled version of the Gaussian variance $\mathbb{V}[\hat{k}_{\text{R}}(\mathbf{x}, \mathbf{y})]$ (15) when using a real Gaussian polynomial sketch Φ_{R} . We have the following relationship:

$$\text{(A)} = 4 \mathbb{V}[A^x A^y] = 4 \times \frac{1}{16} \mathbb{V}[\hat{k}_{\text{R}}(\mathbf{x}, \mathbf{y})] = \frac{1}{4} \mathbb{V}[\hat{k}_{\text{R}}(\mathbf{x}, \mathbf{y})]$$

The factor $1/16$ arises because $\mathbf{a}_i, \mathbf{b}_i \sim \mathcal{N}(\mathbf{0}, \frac{1}{2} \mathbf{I}_d)$ for Φ_{C} . For Φ_{R} we have $\mathbf{a}_i = \text{Re}\{\mathbf{w}_i\} \sim \mathcal{N}(\mathbf{0}, \mathbf{I}_d)$ and $\mathbf{b}_i = \text{Im}\{\mathbf{w}_i\} = \mathbf{0}$ instead (see Section 3.1). This leads to $A_{\text{C}}^x = \frac{1}{2} A_{\text{R}}^x$, $A_{\text{C}}^y = \frac{1}{2} A_{\text{R}}^y$ and finally to $\mathbb{V}[A_{\text{C}}^x A_{\text{C}}^y] = \frac{1}{16} \mathbb{V}[A_{\text{R}}^x A_{\text{R}}^y]$, where C and R refer to the complex and real cases respectively. Having four such terms in the full variance expansion yields the contribution (A) = $\frac{1}{4} \mathbb{V}[\hat{k}_{\text{R}}(\mathbf{x}, \mathbf{y})]$.

(B) = $4 \mathbb{V}[A^x B^y] = \frac{4}{16} \|\mathbf{x}\|^4 \|\mathbf{y}\|^4$ is the contribution of the cross-variance terms $\mathbb{V}[A^x B^y], \mathbb{V}[B^x A^y], \mathbb{V}[C^x D^y]$ and $\mathbb{V}[D^x C^y]$. Finally, (C) is the contribution of all covariance terms. (B) and (C) have the same $\frac{1}{16}$ downscaling as (A).

Futhermore, the following inequality holds:

$$(B) + (C) = \frac{1}{4} \|\mathbf{x}\|^4 \|\mathbf{y}\|^4 + \frac{3}{4} (\mathbf{x}^\top \mathbf{y})^4 \leq (A) = \frac{1}{4} \mathbb{V}[\hat{k}_R(\mathbf{x}, \mathbf{y})] = \frac{1}{4} \|\mathbf{x}\|^4 \|\mathbf{y}\|^4 + \|\mathbf{x}\|^2 \|\mathbf{y}\|^2 (\mathbf{x}^\top \mathbf{y})^2 + \frac{3}{4} (\mathbf{x}^\top \mathbf{y})^2$$

As can be seen from Theorem (4.2), we obtain a *minimal* (zero) variance reduction for CtR-Sketches when $(\mathbf{x}^\top \mathbf{y}) = 0$. In this case, we have $(A) = (B) + (C)$ and therefore $(A) + (B) + (C) = \frac{1}{2} \mathbb{V}[\hat{k}_R(\mathbf{x}, \mathbf{y})]$. CtR-sketches would thus give the same variance as their real analogs when using the *same* number of features as $\mathbb{V}[\hat{k}_R(\mathbf{x}, \mathbf{y})]$ halves in this case. A *maximal* variance reduction is achieved for parallel \mathbf{x} and \mathbf{y} , i.e., $(\mathbf{x}^\top \mathbf{y}) = \|\mathbf{x}\| \|\mathbf{y}\|$ holds. Then we get $(B) + (C) = \frac{1}{2} (A)$ and CtR-sketches thus lead to lower variances *despite* doubling the feature map dimension. The variance reduction of CtR-sketches over their real analogs is thus a mixed effect of the downscaling applied to the variance $\mathbb{V}[\hat{k}_R(\mathbf{x}, \mathbf{y})]$ and the fact that $(B) + (C) \leq (A)$, which is due to the cross-variance and covariance structure produced by CtR polynomial sketches.

Generalizing the analysis to $p > 2$. We saw previously that $(A) = \frac{4}{16} \mathbb{V}[\hat{k}_R(\mathbf{x}, \mathbf{y})]$ for $p = 2$. The computation of (A) can be written as the sum of the variances of the elements of the vector $\mathbf{c} = (A^x, B^x, C^x, D^x)^\top \odot (A^y, B^y, C^y, D^y)^\top$. As shown previously, all 4 variances are equal to $\frac{1}{16} \mathbb{V}[\hat{k}_R(\mathbf{x}, \mathbf{y})]$ leading to an overall downscaling factor of $\frac{4}{16}$ in (A). For general p , the vector \mathbf{c} would contain 2^p non-cross-variance terms and these would be a downscaled version ($1/2^{2p}$) of $\mathbb{V}[\hat{k}_R(\mathbf{x}, \mathbf{y})]$. The downscaling factor is thus $2^p/2^{2p} = 1/2^p$ for arbitrary p . Although we do not compute (B) and (C) for arbitrary p here, we hypothesize that $(B) + (C)$ does not compensate this downscaling (except when $\mathbf{x}^\top \mathbf{y} = 0$) leading to a larger variance reduction for larger p .

B. Further Details about our Proposed TensorSRHT Sketch (Section 5)

One of the main contributions of this work is to propose a structured Rademacher (TensorSRHT) sketch that is a slightly modified version of the TensorSRHT sketch proposed by Ahle et al. (2020) and to propose a CtR-extension of this sketch. Our modification makes it possible to derive the variances of this sketch in closed form, which allows for a direct comparison between CtR-TensorSRHT and its real analog. A closed form variance for TensorSRHT by Ahle et al. (2020) is not available in the literature.

We start by discussing the subtle differences between our version of TensorSRHT and the one by Ahle et al. (2020) in Section B.1 and derive all variances for our sketch in Section B.2. Our variance analysis sheds light onto the statistical advantages of TensorSRHT over Rademacher sketches as discussed in Section 5. As the difference between our sketch and the one by Ahle et al. (2020) is subtle, the insights that we gain from our variance discussion are most likely valid for their sketch as well. We leave an empirical verification of this claim to future work.

B.1. Comparing our version of TensorSRHT to the one proposed in (Ahle et al., 2020)

As mentioned in Section 5, our TensorSRHT sketch can be written in the form of Eq. (3) yielding the complex-valued kernel estimate

$$\hat{k}_C(\mathbf{x}, \mathbf{y}) = \Phi_C(\mathbf{x})^\top \overline{\Phi_C(\mathbf{y})} = \frac{1}{D} \sum_{\ell=1}^D \prod_{i=1}^p (\mathbf{w}_{i,\ell}^\top \mathbf{x}) \overline{(\mathbf{w}_{i,\ell}^\top \mathbf{y})},$$

where the $\{\mathbf{w}_{i,\ell}\}_{\ell=1}^D$ are statistically dependent because each $\mathbf{w}_{i,\ell} = \mathbf{h}_{p_{i,\ell}} \odot \mathbf{d}_i$ depends on the *same* Rademacher vector $\mathbf{d}_i \in \mathbb{C}^d$. $\mathbf{h}_{p_{i,\ell}}^\top$ is the $p_{i,\ell}$ -th row of the Hadamard matrix \mathbf{H} , where the index $p_{i,\ell}$ is the ℓ -th element of the index vector \mathbf{p}_i . This vector is itself obtained by shuffling the vector \mathbf{p}_{base} , a $\lceil D/d \rceil$ -times concatenated version of the vector $(1, \dots, d)^\top$.

We can equivalently write our sketch Φ_C in matrix form as

$$\Phi_C(\mathbf{x}) = ((\mathbf{P}_1 \mathbf{H} \mathbf{D}_1 \mathbf{x}) \odot \dots \odot (\mathbf{P}_p \mathbf{H} \mathbf{D}_p \mathbf{x})) / \sqrt{D},$$

where $\{\mathbf{P}_i\}_{i=1}^p$ are the sampling matrices created from the index vectors $\{\mathbf{p}_i\}_{i=1}^p$ as shown in Section 5. The role of these sampling matrices is to randomly sample D elements from $\{\mathbf{H} \mathbf{D}_i \mathbf{x}\}_{i=1}^p$, where the indices of these elements are contained in the random vectors $\{\mathbf{p}_i\}_{i=1}^p$. Therefore, the ℓ -th element of $\Phi_C(\mathbf{x})$ can be written as

$$\Phi_C(\mathbf{x})_\ell = \frac{1}{\sqrt{D}} \prod_{i=1}^p (\mathbf{H} \mathbf{D}_i \mathbf{x})_{p_{i,\ell}}. \quad (19)$$

Sampling the indices $p_{i,\ell}$ *independently* for each $i \in \{1, \dots, p\}$ (note that they are not independent over $\ell \in \{1, \dots, D\}$) makes it possible to derive the variances of our sketch in closed form.

The sketch by Ahle et al. (2020) uses the same feature constructor as Eq. (19), but uses *dependent* samples $p_{i,\ell}$ over $i \in \{1, \dots, p\}$ and $\ell \in \{1, \dots, D\}$. More precisely, the tuples $(p_{1,\ell}, \dots, p_{p,\ell})$ are sampled from the set $\{1, \dots, d\}^p$ without replacement for every $\ell \in \{1, \dots, D\}$. The sampling procedure by Ahle et al. (2020) can equivalently be described as applying a single sampling matrix $\mathbf{P} \in \mathbb{R}^{D \times d^p}$ (samples are drawn without replacement) to the vectorized outer product $(\mathbf{H}\mathbf{D}_1\mathbf{x} \otimes \dots \otimes \mathbf{H}\mathbf{D}_p\mathbf{x})/\sqrt{D} \in \mathbb{R}^{d^p}$ as shown in (Ahle et al., 2020, Definition 15).

The approach by Ahle et al. (2020) and ours are equivalent for $D \leq d$. They differ slightly for $D > d$ as it becomes possible to sample two equal index tuples $(p_{1,\ell}, \dots, p_{p,\ell})$ for $\ell \neq \ell'$ using our method because these tuples are sampled independently over $i \in \{1, \dots, p\}$ and therefore not fully without replacement (only ℓ is sampled without replacement for each i). However, since the space of possible tuples $(p_{1,\ell}, \dots, p_{p,\ell})$ is d^p -dimensional, obtaining equal tuples occurs rarely in practice when using our method, especially when d or p are moderately large.

B.2. Variances of our version of TensorSRHT as well as CtR-TensorSRHT

As shown in Section A.1, the variance of the CtR polynomial sketches discussed in this work is of the form:

$$\mathbb{V}[\hat{k}_{\text{CtR}}(\mathbf{x}, \mathbf{y})] = \frac{1}{2}(\mathbb{V}[\hat{k}_{\text{C}}(\mathbf{x}, \mathbf{y})] + \mathbb{P}\mathbb{V}[\hat{k}_{\text{C}}(\mathbf{x}, \mathbf{y})]),$$

where $\hat{k}_{\text{C}}(\mathbf{x}, \mathbf{y})$ is the complex-valued kernel estimate of the polynomial kernel obtained through our sketch. In order to derive the variance of CtR-TensorSRHT, we need to derive the variance $\mathbb{V}[\hat{k}_{\text{C}}(\mathbf{x}, \mathbf{y})]$ and the pseudo-variance $\mathbb{P}\mathbb{V}[\hat{k}_{\text{C}}(\mathbf{x}, \mathbf{y})]$. We will also derive the variance of real-valued TensorSRHT as a corollary of the variance of complex TensorSRHT.

B.2.1. PSEUDO-VARIANCE

As before, we start with the pseudo-variance and derive the variance after. For the pseudo-variance $\mathbb{P}\mathbb{V}[\hat{k}_{\text{C}}(\mathbf{x}, \mathbf{y})] = \mathbb{E}[\hat{k}_{\text{C}}(\mathbf{x}, \mathbf{y})^2] - \mathbb{E}[\hat{k}_{\text{C}}(\mathbf{x}, \mathbf{y})]^2$, we need to work out $\mathbb{E}[\hat{k}_{\text{C}}(\mathbf{x}, \mathbf{y})^2]$:

$$\mathbb{E}[\hat{k}_{\text{C}}(\mathbf{x}, \mathbf{y})^2] = \frac{1}{D^2} \sum_{\ell=1}^D \sum_{\ell'=1}^D \prod_{i=1}^p \mathbb{E} \left[(\mathbf{w}_{i,\ell}^\top \mathbf{x})(\overline{\mathbf{w}_{i,\ell}^\top \mathbf{y}})(\mathbf{w}_{i,\ell'}^\top \mathbf{x})(\overline{\mathbf{w}_{i,\ell'}^\top \mathbf{y}}) \right] = \frac{1}{D^2} \sum_{\ell=1}^D \sum_{\ell'=1}^D \underbrace{\mathbb{E} \left[(\mathbf{w}_\ell^\top \mathbf{x})(\overline{\mathbf{w}_\ell^\top \mathbf{y}})(\mathbf{w}_{\ell'}^\top \mathbf{x})(\overline{\mathbf{w}_{\ell'}^\top \mathbf{y}}) \right]^p}_{e(\ell, \ell')^p}$$

We dropped the index i in the last equality for ease of notation, as all $\{\mathbf{w}_{i,\ell}\}_{i=1}^p$ are i.i.d. samples and the expectation is thus the same for any i . To work out the expectation $e(\ell, \ell')$, we need to distinguish different cases for ℓ and ℓ' .

1. $\ell = \ell'$ (D terms): $e(\ell, \ell')^p = \mathbb{E} \left[(\mathbf{w}_\ell^\top \mathbf{x})^2 (\overline{\mathbf{w}_\ell^\top \mathbf{y}})^2 \right]^p = \left(2(\mathbf{x}^\top \mathbf{y}^2) - \sum_{i=1}^d x_i^2 y_i^2 \right)^p$
(taken from Eq. (11) for the Rademacher case)
2. $\ell \neq \ell'$ ($D(D-1)$ terms):

$$\begin{aligned} e(\ell, \ell')^p &= \left(\sum_{q=1}^d \sum_{r=1}^d \sum_{s=1}^d \sum_{t=1}^d \mathbb{E} [w_{\ell,q} \overline{w_{\ell,r}} w_{\ell',s} \overline{w_{\ell',t}}] x_q y_r x_s y_t \right)^p \\ &= \left(\sum_{q=1}^d \sum_{r=1}^d \sum_{s=1}^d \sum_{t=1}^d \mathbb{E} [d_q \overline{d_r} d_s \overline{d_t}] \mathbb{E} [h_{p_\ell, q} h_{p_\ell, r} h_{p_{\ell'}, s} h_{p_{\ell'}, t}] x_q y_r x_s y_t \right)^p \end{aligned}$$

d_q, d_r, d_s, d_t are uniform samples from $\{1, -1, i, -i\}$, i.e., complex Rademacher samples, that are independent from the index samples $p_{\ell,q}, p_{\ell,r}, p_{\ell',s}, p_{\ell',t}$, which is why we can factor out the two expectations. We will simplify the above sum by studying when $\mathbb{E}[d_q \overline{d_r} d_s \overline{d_t}] \neq 0$.

We have to distinguish three non-zero cases for $\mathbb{E}[d_q \overline{d_r} d_s \overline{d_t}]$:

1. $q = r = s = t$ (d terms): $\mathbb{E}[d_q \overline{d_r} d_s \overline{d_t}] = \mathbb{E}[|d_q|^4] = 1$

2. $q = r \neq s = t$ ($d(d-1)$ terms): $\mathbb{E}[d_q \overline{d_r} d_s \overline{d_t}] = \mathbb{E}[|d_q|^2] \mathbb{E}[|d_s|^2] = 1$

3. $q = t \neq r = s$ ($d(d-1)$ terms): $\mathbb{E}[d_q \overline{d_r} d_s \overline{d_t}] = \mathbb{E}[|d_q|^2] \mathbb{E}[|d_r|^2] = 1$

because $\mathbb{E}[|d_q|^4] = \mathbb{E}[|d_q|^2] = 1$.

In Section B.2.3, we show that for $\ell \neq \ell'$ and $q \neq r$, $\mathbb{E}[h_{p_\ell, q} h_{p_\ell, r} h_{p_{\ell'}, r} h_{p_{\ell'}, q}] = -\frac{1}{\lceil D/d \rceil d - 1}$ holds. Therefore, $e(\ell, \ell')^p$ for $\ell \neq \ell'$ yields:

$$\begin{aligned} e(\ell, \ell')^p &= \left(\sum_{i=1}^d x_i^2 y_i^2 + \sum_{i=1}^d \sum_{j \neq i}^d x_i y_i x_j y_j - \frac{1}{\lceil D/d \rceil d - 1} \sum_{i=1}^d \sum_{j \neq i}^d x_i y_i x_j y_j \right)^p \\ &= \left((\mathbf{x}^\top \mathbf{y})^2 - \frac{1}{\lceil D/d \rceil d - 1} \left[(\mathbf{x}^\top \mathbf{y})^2 - \sum_{i=1}^d x_i^2 y_i^2 \right] \right)^p \end{aligned}$$

In fact, $e(\ell, \ell')^p$ does not depend on ℓ and ℓ' anymore after working out the expectations involved. Plugging $e(\ell, \ell')^p$ back into $\mathbb{E}[\hat{k}_C(\mathbf{x}, \mathbf{y})^2]$ yields the following pseudo-variance for TensorSRHT:

$$\begin{aligned} \mathbb{P}\mathbb{V}[\hat{k}_C(\mathbf{x}, \mathbf{y})^2] &= \frac{1}{D} \left[\left(2(\mathbf{x}^\top \mathbf{y})^2 - \sum_{i=1}^d x_i^2 y_i^2 \right)^p - (\mathbf{x}^\top \mathbf{y})^{2p} \right] \\ &\quad + \left(1 - \frac{1}{D} \right) \left[\left((\mathbf{x}^\top \mathbf{y})^2 - \frac{1}{\lceil D/d \rceil d - 1} \left[(\mathbf{x}^\top \mathbf{y})^2 - \sum_{i=1}^d x_i^2 y_i^2 \right] \right)^p - (\mathbf{x}^\top \mathbf{y})^{2p} \right] \\ &= \frac{1}{D} \mathbb{P}\mathbb{V}_{\text{Rad.}}^{(p)} - \left(1 - \frac{1}{D} \right) \left[(\mathbf{x}^\top \mathbf{y})^{2p} - \left((\mathbf{x}^\top \mathbf{y})^2 - \frac{\mathbb{P}\mathbb{V}_{\text{Rad.}}^{(1)}}{\lceil D/d \rceil d - 1} \right)^p \right] \end{aligned} \quad (20)$$

$\mathbb{P}\mathbb{V}_{\text{Rad.}}^{(p)}$ and $\mathbb{P}\mathbb{V}_{\text{Rad.}}^{(1)}$ are the Rademacher pseudo-variance (13) for a given degree p and $p = 1$, respectively.

B.2.2. VARIANCE

Next we work out the variance $\mathbb{V}[\hat{k}_C(\mathbf{x}, \mathbf{y})]$:

$$\mathbb{V} \left[\frac{1}{D} \sum_{\ell=1}^D \prod_{i=1}^p (\mathbf{w}_{i,\ell}^\top \mathbf{x}) (\overline{\mathbf{w}_{i,\ell}^\top \mathbf{y}}) \right] = \frac{1}{D^2} \sum_{\ell=1}^D \sum_{\ell'=1}^D \text{Cov} \left(\prod_{i=1}^p (\mathbf{w}_{i,\ell}^\top \mathbf{x}) (\overline{\mathbf{w}_{i,\ell}^\top \mathbf{y}}), \prod_{i=1}^p (\mathbf{w}_{i,\ell'}^\top \mathbf{x}) (\overline{\mathbf{w}_{i,\ell'}^\top \mathbf{y}}) \right)$$

Again, we distinguish the cases $\ell = \ell'$ and $\ell \neq \ell'$:

1. $\ell = \ell'$ (D terms):

$$\begin{aligned} \text{Cov} \left(\prod_{i=1}^p (\mathbf{w}_{i,\ell}^\top \mathbf{x}) (\overline{\mathbf{w}_{i,\ell}^\top \mathbf{y}}), \prod_{i=1}^p (\mathbf{w}_{i,\ell}^\top \mathbf{x}) (\overline{\mathbf{w}_{i,\ell}^\top \mathbf{y}}) \right) &= \mathbb{V} \left[\prod_{i=1}^p (\mathbf{w}_{i,\ell}^\top \mathbf{x}) (\overline{\mathbf{w}_{i,\ell}^\top \mathbf{y}}) \right] \\ &= \left(\|\mathbf{x}\|^2 \|\mathbf{y}\|^2 + (\mathbf{x}^\top \mathbf{y})^2 - \sum_{i=1}^d x_i^2 y_i^2 \right)^p - (\mathbf{x}^\top \mathbf{y})^{2p} \quad (\text{Using the complex Rademacher variance (16)}) \end{aligned}$$

2. $\ell \neq \ell'$ ($D(D-1)$ terms). We discuss this case in detail below.

$$\begin{aligned} \text{Cov} \left(\prod_{i=1}^p (\mathbf{w}_{i,\ell}^\top \mathbf{x}) (\overline{\mathbf{w}_{i,\ell}^\top \mathbf{y}}), \prod_{i=1}^p (\mathbf{w}_{i,\ell'}^\top \mathbf{x}) (\overline{\mathbf{w}_{i,\ell'}^\top \mathbf{y}}) \right) &= \mathbb{E} \left[\prod_{i=1}^p (\mathbf{w}_{i,\ell}^\top \mathbf{x}) (\overline{\mathbf{w}_{i,\ell}^\top \mathbf{y}}) (\overline{\mathbf{w}_{i,\ell'}^\top \mathbf{x}}) (\mathbf{w}_{i,\ell'}^\top \mathbf{y}) \right] - (\mathbf{x}^\top \mathbf{y})^{2p} \quad (21) \\ &= \mathbb{E} \left[(\mathbf{w}_\ell^\top \mathbf{x}) (\overline{\mathbf{w}_\ell^\top \mathbf{y}}) (\overline{\mathbf{w}_{\ell'}^\top \mathbf{x}}) (\mathbf{w}_{\ell'}^\top \mathbf{y}) \right]^p - (\mathbf{x}^\top \mathbf{y})^{2p} = \underbrace{\mathbb{E} \left[(\mathbf{w}_\ell^\top \mathbf{x}) (\overline{\mathbf{w}_\ell^\top \mathbf{y}}) (\overline{\mathbf{w}_{\ell'}^\top \mathbf{x}}) (\mathbf{w}_{\ell'}^\top \mathbf{y}) \right]^p}_{e_2(\ell, \ell')^p} - (\mathbf{x}^\top \mathbf{y})^{2p} \end{aligned}$$

Next, we turn to the expression $e_2(\ell, \ell')^p$ that is almost the same as $e(\ell, \ell')^p$ for the pseudo-variance, the only difference being the complex conjugates that are placed differently:

$$\begin{aligned} e_2(\ell, \ell')^p &= \left(\sum_{q=1}^d \sum_{r=1}^d \sum_{s=1}^d \sum_{t=1}^d \mathbb{E}[w_{\ell,q} \overline{w_{\ell,r} w_{\ell',s} w_{\ell',t}}] x_q y_r x_s y_t \right)^p \\ &= \left(\sum_{q=1}^d \sum_{r=1}^d \sum_{s=1}^d \sum_{t=1}^d \mathbb{E}[d_q \overline{d_r d_s d_t}] \mathbb{E}[h_{p_\ell,q} h_{p_\ell,r} h_{p_{\ell'},s} h_{p_{\ell'},t}] x_q y_r x_s y_t \right)^p \end{aligned}$$

We distinguish 4 cases for $\mathbb{E}[d_q \overline{d_r d_s d_t}]$:

1. $q = r = s = t$ (d terms): $\mathbb{E}[d_q \overline{d_r d_s d_t}] = \mathbb{E}[|d_q|^4] = 1$
2. $q = r \neq s = t$ ($d(d-1)$ terms): $\mathbb{E}[d_q \overline{d_r d_s d_t}] = \mathbb{E}[|d_q|^2] \mathbb{E}[|d_s|^2] = \mathbb{E}[|d_q|^2]^2 = 1$
3. $q = s \neq r = t$ ($d(d-1)$ terms): $\mathbb{E}[d_q \overline{d_r d_s d_t}] = \mathbb{E}[|d_q|^2] \mathbb{E}[|d_r|^2] = \mathbb{E}[|d_q|^2]^2 = 1$
4. $q = t \neq r = s$ ($d(d-1)$ terms): $\mathbb{E}[d_q \overline{d_r d_s d_t}] = \mathbb{E}[d_q^2] \mathbb{E}[\overline{d_r^2}] = 0$

We showed case (4) on purpose although it is zero for complex Rademacher samples $d_q, d_r \in \mathbb{C}$. For real Rademacher samples, we have $\mathbb{E}[d_q^2] = \mathbb{E}[\overline{d_r^2}] = 1$ instead. This observation will allow us to work out the variance of complex and real TensorSRHT at the same time. Furthermore, we have $\mathbb{E}[h_{p_\ell,q} h_{p_\ell,r} h_{p_{\ell'},s} h_{p_{\ell'},t}] = -\frac{1}{\lceil D/d \rceil d}$ for any $q \neq r$ and $\ell \neq \ell'$ as already noted for the pseudo-variance. The derivation of this quantity is shown in Section B.2.3.

So $e_2(\ell, \ell')$ reduces to:

$$\begin{aligned} e_2(\ell, \ell') &= \underbrace{\sum_{i=1}^d x_i^2 y_i^2}_{\text{Case (1)}} + \underbrace{\sum_{i=1}^d \sum_{j \neq i}^d x_i x_j y_i y_j}_{\text{Case (2)}} - \underbrace{\frac{1}{\lceil D/d \rceil d} \sum_{i=1}^d \sum_{j \neq i}^d x_i^2 y_j^2}_{\text{Case (3)}} - \underbrace{\frac{1}{\lceil D/d \rceil d} \sum_{i=1}^d \sum_{j \neq i}^d \mathbb{E}[d_i^2] \mathbb{E}[\overline{d_j^2}] x_i x_j y_i y_j}_{\text{Case (4)}} \\ &= (\mathbf{x}^\top \mathbf{y})^2 - \frac{1}{\lceil D/d \rceil d} \sum_{i=1}^d \sum_{j \neq i}^d x_i^2 y_j^2 + \mathbb{E}[d_i^2] x_i x_j y_i y_j, \end{aligned}$$

where $\mathbb{E}[d_i^2] = 0$ for the complex case and $\mathbb{E}[d_i^2] = 1$ for the real case. Plugging back $e_2(\ell, \ell')$ for the case $\ell \neq \ell'$ back into Eq. (21) and solving for $\mathbb{V}[\hat{k}_C(\mathbf{x}, \mathbf{y})]$ yields:

$$\mathbb{V}[\hat{k}_C(\mathbf{x}, \mathbf{y})] = \mathbb{V}_{\text{Rad.}}^{(p)} - \left(1 - \frac{1}{D}\right) \left[(\mathbf{x}^\top \mathbf{y})^{2p} - \left((\mathbf{x}^\top \mathbf{y})^2 - \frac{\mathbb{V}_{\text{Rad.}}^{(1)}}{\lceil D/d \rceil d - 1} \right)^p \right] \quad (22)$$

with $\mathbb{V}_{\text{Rad.}}^{(p)}$ and $\mathbb{V}_{\text{Rad.}}^{(1)}$ being the Rademacher variance (16) for a given degree p and $p = 1$, respectively. We set $q = 2$ for the real case and $q = 1$ for the complex case inside Eq. (16).

Inserting the expressions for the variance (22) and pseudo-variance (20) into Eq. (6), gives the variance of Ctr-TensorSRHT.

B.2.3. SHUFFLING THE ROWS OF STACKED HADAMARD MATRICES

In this section, we prove an important equality that was used in the derivation of the variance formulas of TensorSRHT in the previous sections. It can be seen as the key lemma that leads to a reduced variance compared to Rademacher sketches. It shows the statistics of randomly sampled rows (without replacement) inside stacked orthogonal Hadamard matrices that give close-to-orthogonal as opposed to i.i.d. samples in our proposed TensorSRHT sketch. We prove the equality

$$\mathbb{E}[h_{p_\ell,q} h_{p_\ell,r} h_{p_{\ell'},s} h_{p_{\ell'},t}] = -\frac{1}{\lceil D/d \rceil d - 1}$$

for $\ell \neq \ell'$ and $q \neq r$ being fixed indices. $\mathbf{h}_{p_\ell}^\top$ and $\mathbf{h}_{p_{\ell'}}^\top$ are the p_ℓ -th and $p_{\ell'}$ -th row of the Hadamard matrix \mathbf{H} , respectively as shown in Section 5. The indices q and r refer to elements inside these row vectors. p_ℓ and $p_{\ell'}$ are themselves the ℓ -th and ℓ' -th entries of the random vector $\mathbf{p}_i \in \mathbb{R}^{\lceil D/d \rceil d}$ for a given $i \in \{1, \dots, p\}$ (we look at a given index i above and drop the index for ease of presentation). They are used to construct the sampling matrices $\{\mathbf{P}_i\}_{i=1}^p$ in Section 5. Recall that the vectors $\{\mathbf{p}_i\}_{i=1}^p$ are obtained by shuffling the vector \mathbf{p}_{base} , a $\lceil D/d \rceil$ -times concatenation of $(1, \dots, d)^\top \in \mathbb{R}^d$.

The following proof is closely related to Choromanski et al. (2017, Proof of Proposition 8.2) and Wacker et al. (2022, Lemma B.1). The difference here is that we consider the sampling of rows (without replacement) inside *stacked* Hadamard matrices as we will see next, whereas the other works only consider the sampling of rows inside a *single* Hadamard matrix.

Proof

The sampling procedure for the rows $\mathbf{h}_{p_\ell}^\top$ and $\mathbf{h}_{p_{\ell'}}^\top$ can be described as follows. We stack the Hadamard matrix $\mathbf{H} \in \mathbb{R}^{d \times d}$ $\lceil D/d \rceil$ times on top of itself to yield a new matrix $\mathbf{H}^{\lceil D/d \rceil} \in \mathbb{R}^{\lceil D/d \rceil d \times d}$. We then shuffle its rows randomly to yield the shuffled matrix $\mathbf{H}_\mathbf{p}^{\lceil D/d \rceil}$. $\mathbf{h}_{p_\ell}^\top$ and $\mathbf{h}_{p_{\ell'}}^\top$ are then the ℓ -th and ℓ' -th row of $\mathbf{H}_\mathbf{p}^{\lceil D/d \rceil}$. In fact, the shuffled matrix $\mathbf{H}_\mathbf{p}^{\lceil D/d \rceil}$ can be constructed from the index vector \mathbf{p} that contains the order of the rows of \mathbf{H} to be used.

Since the columns of \mathbf{H} are orthogonal, the same is true for $\mathbf{H}^{\lceil D/d \rceil}$ and $\mathbf{H}_\mathbf{p}^{\lceil D/d \rceil}$. So the inner product of two distinct columns q and r of $\mathbf{H}_\mathbf{p}^{\lceil D/d \rceil}$ yields $\sum_{\ell=1}^{\lceil D/d \rceil} h_{p_\ell, q} h_{p_\ell, r} = 0$. As $h_{p_\ell, q}, h_{p_\ell, r} \in \{1, -1\}$, half of $\{h_{p_\ell, q} h_{p_\ell, r}\}_{\ell=1}^{\lceil D/d \rceil}$ must be equal to 1 and -1 , respectively. From this we get the marginal probabilities

$$\Pr(h_{p_\ell, q} h_{p_\ell, r} = 1) = \Pr(h_{p_\ell, q} h_{p_\ell, r} = -1) = 0.5$$

for any $q \neq r$ being fixed, where the probabilities are taken over the indices p_ℓ and $p_{\ell'}$, i.e., the shuffling operation. Next, we obtain the following conditional probabilities using the same logic as before:

$$\begin{aligned} \Pr(h_{\ell', q} h_{\ell', r} = 1 | h_{\ell, q} h_{\ell, r} = 1) &= \Pr(h_{\ell', q} h_{\ell', r} = -1 | h_{\ell, q} h_{\ell, r} = -1) = \frac{(\lceil D/d \rceil d)/2 - 1}{\lceil D/d \rceil d - 1} \\ \Pr(h_{\ell', q} h_{\ell', r} = 1 | h_{\ell, q} h_{\ell, r} = -1) &= \Pr(h_{\ell', q} h_{\ell', r} = -1 | h_{\ell, q} h_{\ell, r} = 1) = \frac{(\lceil D/d \rceil d)/2}{\lceil D/d \rceil d - 1} \end{aligned}$$

Using these conditional probabilities along with the marginal probabilities $\Pr(h_{p_\ell, q} h_{p_\ell, r})$ allows us to solve $\mathbb{E}[h_{p_\ell, q} h_{p_\ell, r} h_{p_{\ell'}, r} h_{p_{\ell'}, q}]$ via the law of total expectation:

$$\begin{aligned} \mathbb{E}[h_{p_\ell, q} h_{p_\ell, r} h_{p_{\ell'}, r} h_{p_{\ell'}, q}] &= \mathbb{E}_{p_\ell} [\mathbb{E}_{p_{\ell'}} [h_{p_\ell, q} h_{p_\ell, r} h_{p_{\ell'}, r} h_{p_{\ell'}, q} | h_{p_\ell, r} h_{p_\ell, q}]] \\ &= \frac{1}{2} (\mathbb{E}_{p_{\ell'}} [h_{p_{\ell'}, r} h_{p_{\ell'}, q} | h_{p_\ell, r} h_{p_\ell, q} = 1] - \mathbb{E}_{p_{\ell'}} [h_{p_{\ell'}, r} h_{p_{\ell'}, q} | h_{p_\ell, r} h_{p_\ell, q} = -1]) \\ &= \frac{1}{2} \left(\left(\frac{(\lceil D/d \rceil d)/2 - 1}{\lceil D/d \rceil d - 1} - \frac{(\lceil D/d \rceil d)/2}{\lceil D/d \rceil d - 1} \right) - \left(\frac{(\lceil D/d \rceil d)/2}{\lceil D/d \rceil d - 1} - \frac{(\lceil D/d \rceil d)/2 - 1}{\lceil D/d \rceil d - 1} \right) \right) \\ &= -\frac{1}{\lceil D/d \rceil d - 1} \end{aligned}$$

■

C. Further Experiments

C.1. Variance Comparisons

Fig. (5) shows the results of the same experiment as Fig. (1a), but for CtR-Rademacher sketches compared with their real analogs. We study the practical effect of the non-negativity condition in Theorem (4.1). Fig. (5a) shows the case where the condition $a = \sum_{i=1}^d \sum_{j \neq i} x_i x_j y_i y_j \geq 0$ always holds and Fig. (5b) the case, where $a \geq 0$ does not always hold as the data is zero-centered. We see that the condition is needed to guarantee an advantage of the CtR sketch while the CtR sketch offers lower variance ratios for CIFAR-10 and MNIST in most cases even if $a \geq 0$ does not always hold. For Letter and Mocap, around half the variances ratios are less than one and half are more than one, suggesting that real Rademacher sketches perform similarly to CtR-Rademacher sketches in this case.

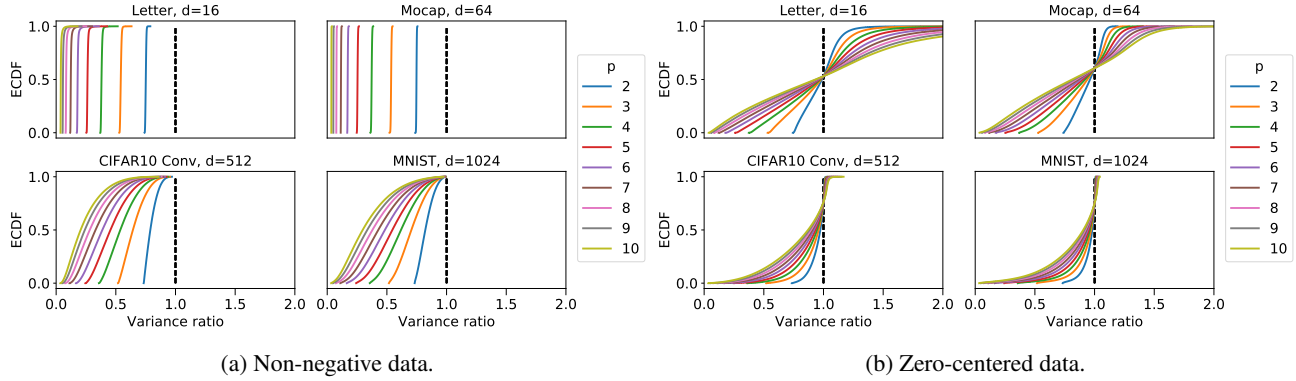


Figure 5. ECDF of $\text{Var}(\text{CtR-Rademacher}) / \text{Var}(\text{Rademacher})$ for pairwise evaluations of the variance ratio evaluated on a subset of each dataset.

Fig. (6a) shows the results of the same CtR-TensorSRHT experiment as in Fig. (1a), but this time on zero-centered data, where the condition a does not always hold. In this case, roughly half of the variance ratios are below and above 1, respectively. Thus CtR-TensorSRHT performs similarly compared to real TensorSRHT on all datasets. The non-negativity condition is therefore as beneficial for CtR-TensorSRHT as for CtR-Rademacher sketches. This makes sense because both the variance and the pseudo-variance of TensorSRHT are closely related to the ones of Rademacher sketches as shown in Table (1).

Fig. (6b) shows a comparison of TensorSRHT without the CtR-extension against TensorSketch. We can see that the results are much worse than for the CtR case in Fig. (1b). Only degrees one and two have lower variance ratios. This comparison underlines the necessity of CtR-extensions.

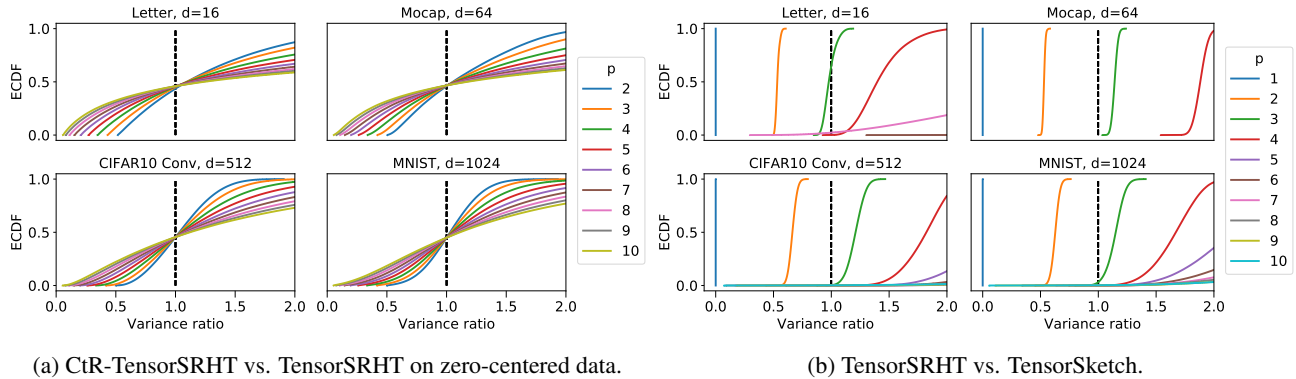


Figure 6. Empirical cumulative distribution function of variance ratios for feature maps with equal dimension $D = 2d$. The target kernel is $(\mathbf{x}^\top \mathbf{y} + 1)^p$.

C.2. Time Benchmarks

Fig. (7) shows the same experiment as Fig. (2) but for the polynomial degree $p = 3$. CtR-TensorSRHT and TensorSRHT are still faster than TensorSketch for $D > d$. CtR-TensorSRHT has a smaller advantage over real TensorSRHT as for $p = 6$ regarding kernel approximation errors.

Fig. (8) shows the results of a stochastic variational inference experiment to obtain a factorized Gaussian posterior distribution over the weights of a GP classifier. We show test error vs. training time with $D = 10d$ random features on the MNIST dataset. The feature maps approximate the kernel $(\gamma \mathbf{x}^\top \mathbf{y} + \nu)^6$, where $\gamma, \nu \geq 0$ are optimized through backpropagation. The mini-batch size was chosen to be 1000 and we used the Adam optimizer with learning rate 10^{-3} . We choose 50 Monte-Carlo samples for the posterior weights at each iteration. When using TensorSRHT, the experiments were run for 150 epochs while the ones for TensorSketch were run for 50 epochs. We can see that we achieve a much faster convergence (in wall-clock time) using TensorSRHT, which is due to a faster computation of the feature map as shown in

Fig. (2). CtR-TensorSRHT outperforms TensorSRHT and is only slightly slower.

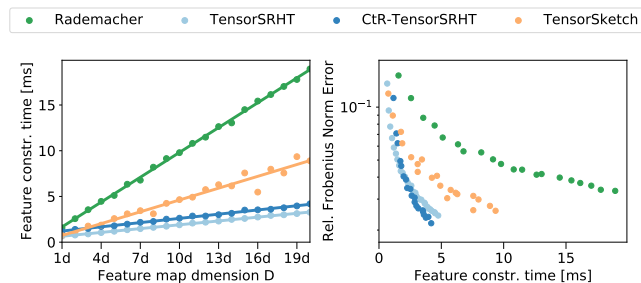


Figure 7. (Left) Feature construction time against feature map dimension D . (Right) Kernel approximation error (rel. Frobenius norm error) against feature construction time. We approximate the kernel $k(\mathbf{x}, \mathbf{y}) = (\mathbf{x}^\top \mathbf{y} + 1)^3$ on 1000 random MNIST samples.

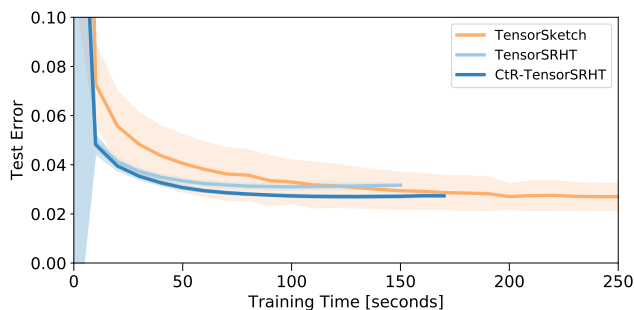


Figure 8. Stochastic variational inference on MNIST ($d = 1024$) for $D = 10d$ and $p = 6$. Results are averaged over 10 different runs.

C.3. Closed-Form GP Classification

We carry out a set of additional GP classification experiments, where the classification is modeled as a closed-form regression problem using transformed labels as described in Milios et al. (2018). The experiments are the same as in Fig. (3), but use different polynomial kernels as well as differently scaled data. We also add two more datasets (Letter and Mocap (Dua & Graff, 2017)) that we left out for space reasons before.

Fig. (10) is the same as Fig. (3), but showing *all* datasets this time.

Fig. (11) is the same as Fig. (10), but using $p = 6$ instead of $p = 3$. The higher polynomial degree leads to a larger relative improvement of CtR-sketches over their real analogs for all studied metrics. The relative improvement of CtR-TensorSRHT compared to TensorSketch is lower than for $p = 3$.

Fig. (12) shows the same experiment as before, but for zero-centered data to break the non-negativity condition of Theorem (4.1). The relative advantage of CtR polynomial sketches over their real analogs decreases in this case except for Gaussian sketches. Nonetheless, an advantage remains even in this case suggesting that CtR-sketches should always be preferred.

Fig. (13) and (14) show the same experiments as before for degrees $p = 3$ and $p = 6$, but this time with min-max feature scaling instead of unit-normalization applied to the data. In this case, we choose $\gamma = 1/d$ for the polynomial kernel. CtR polynomial sketches obtain larger relative gains over TensorSketch than for unit-normalized data. The relative advantage of CtR over real-valued sketches decreases. The reason is that the polynomial kernel parameterization places more weight on low polynomial degrees that favor TensorSRHT but have a lower CtR benefit.

C.4. MMD experiments

In this section, we compare the approximation of the *Kernel Inception Distance (KID)* (Bińkowski et al., 2018). This distance is used to measure the similarity between two datasets (a lower distance refers to a higher similarity).

KID corresponds to the squared MMD (Gretton et al., 2012) using the polynomial kernel $(\frac{1}{d}x^\top y + 1)^p$, where this kernel is computed on top of the convolutional features obtained through the Inception (Szegedy et al., 2016) neural network architecture.

As the computation of the MMD metric scales quadratically in the number of datapoints, approximation methods have to be used for large datasets such as CIFAR-10 that we use here.

We follow the experiment in the original work (Bińkowski et al., 2018), which uses the average of blockwise MMD values (Block-MMD) as an approximation. In this case, the exact squared MMD is computed on a subset of size n of each dataset and this process is repeated for 100 independent subset samples. We then compute the standard deviation of these samples. Block-MMD will serve as our baseline and we use $n \in \{100, 1000, 5000, 10000, 15000, 20000\}$.

We compare this baseline against squared MMD estimates obtained through polynomial sketches. We obtain unbiased squared MMD estimates using the method described in Sutherland & Schneider (2015, Section 3). We repeat this process 100 times as before and compute the standard deviation on the estimate. We use $D \in \{64, 128, 256, 512, 1024, d, 2d, 3d, 4d\}$ in our experiments, where $d = 2048$.

Fig. (9) shows the standard deviation of the squared MMD (KID) estimates computed as explained before. We see that all polynomial sketches achieve around one order of magnitude lower standard deviations than the Block-MMD baseline in the same computation time. TensorSRHT and CtR-TensorSRHT perform slightly better than TensorSketch for $p = 3$ and CtR-TensorSRHT performs better for $p = 6$. However, the differences between the polynomial sketches are not as large as for the kernel approximation errors in Fig. (13) and (14), where the same target kernel is used.

Table (2) shows the same standard deviations as before but computed on 1000 instead of 100 resamples of the KID metric. The results are thus more accurate. However, obtaining these more accurate estimates is slower and therefore less samples are used in practice.

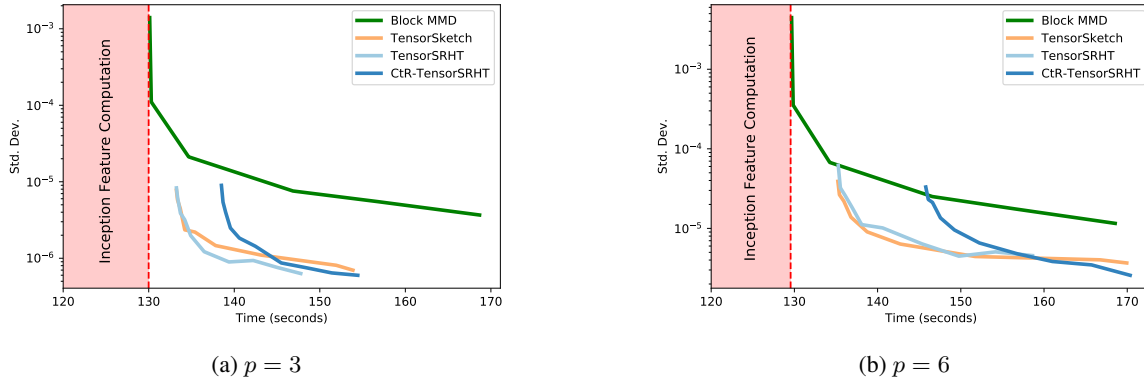


Figure 9. Standard deviation of the KID estimator between the CIFAR-10 train and test sets estimated on 100 independent resamples of the metric. Note that the first 130 seconds are spent on computing the Inception features (the plot starts at 120 to become better readable).

Table 2. Standard deviation of the KID estimator between the CIFAR-10 train and test sets estimated on 1000 independent samples.

	$p = 3$				$p = 6$			
	$D = 1d$	$D = 2d$	$D = 3d$	$D = 4d$	$D = 1d$	$D = 2d$	$D = 3d$	$D = 4d$
TensorSketch	1.363E-06	9.639E-07	7.837E-07	6.841E-07	6.974E-06	4.909E-06	4.015E-06	3.436E-06
TensorSRHT	1.435E-06	1.047E-06	7.869E-07	6.946E-07	9.476E-06	6.897E-06	5.331E-06	4.871E-06
CtR-TensorSRHT	1.312E-06	8.747E-07	7.420E-07	5.941E-07	6.697E-06	4.856E-06	3.762E-06	3.260E-06

Complex-to-Real Random Features for Polynomial Kernels

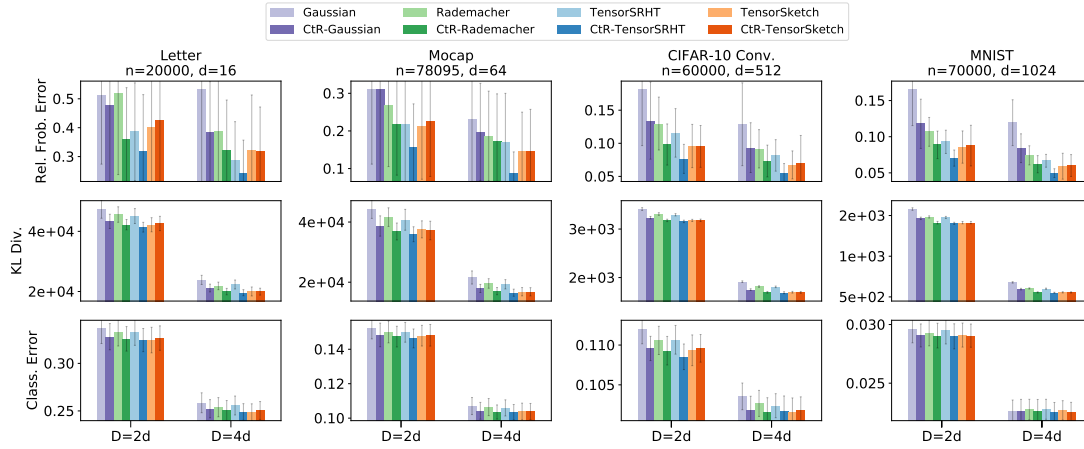


Figure 10. Gaussian Process classification experiments comparing different polynomial sketches along with their CtR extensions for $D \in \{2d, 4d\}$. The target polynomial kernel is $(\mathbf{x}^\top \mathbf{y} + 1)^3$ and the data is unit-normalized.

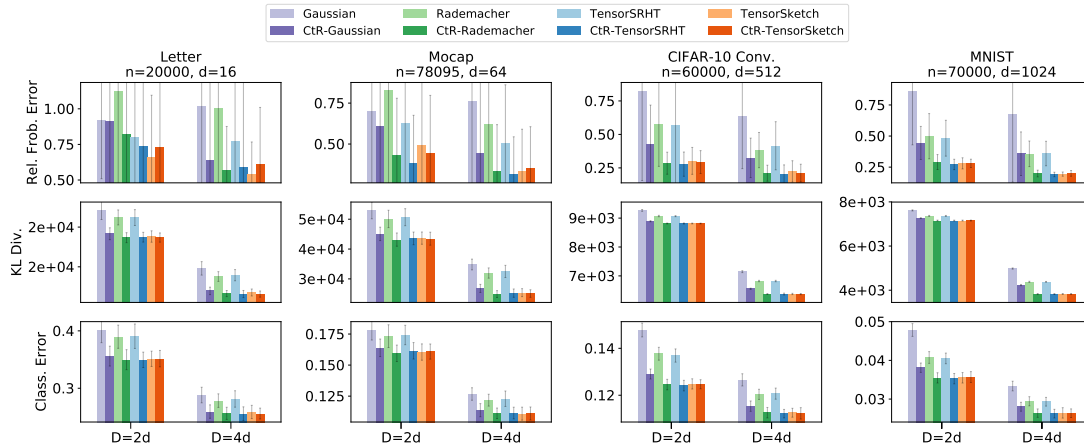


Figure 11. Gaussian Process classification experiments comparing different polynomial sketches along with their CtR extensions for $D \in \{2d, 4d\}$. The target polynomial kernel is $(\mathbf{x}^\top \mathbf{y} + 1)^6$ and the data is unit-normalized.

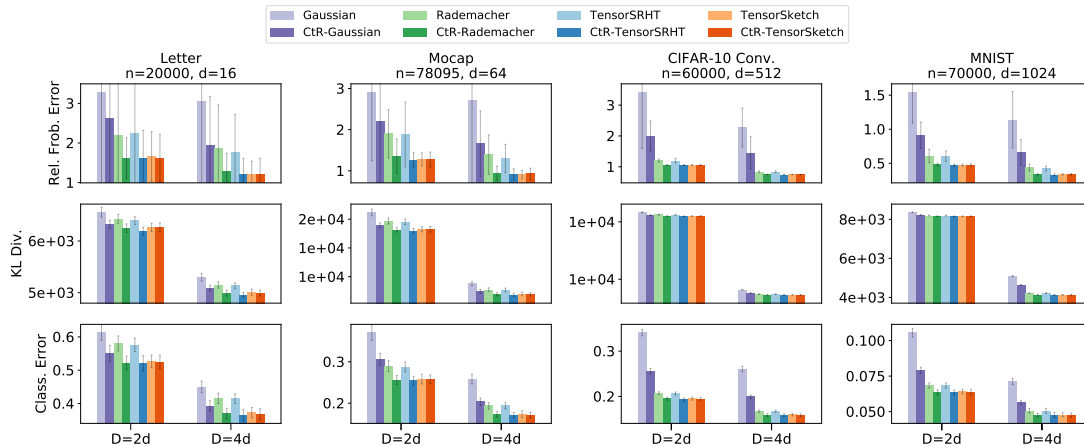


Figure 12. Gaussian Process classification experiments comparing different polynomial sketches along with their CtR-extensions for $D \in \{2d, 4d\}$. The target polynomial kernel is $(\mathbf{x}^\top \mathbf{y} + 1)^6$ and the data is unit-normalized as well as zero-centered.

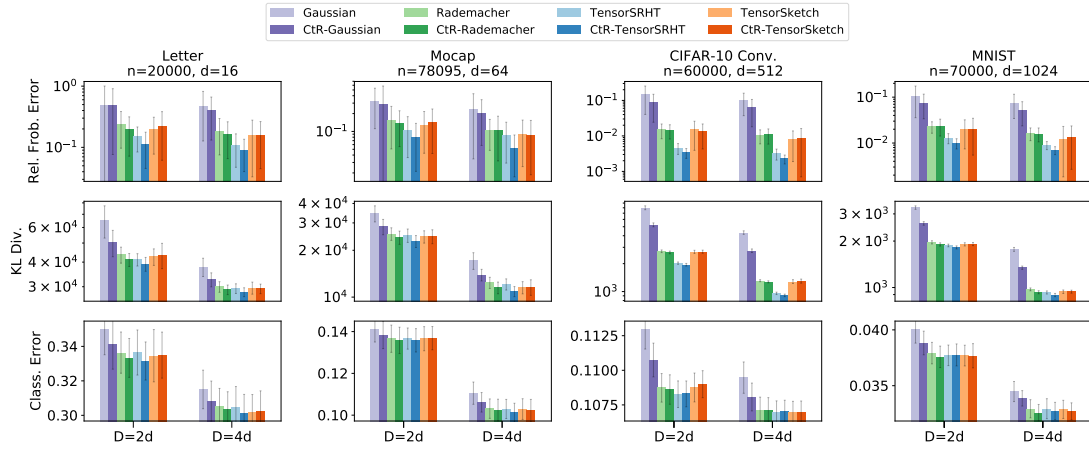


Figure 13. Gaussian Process classification experiments comparing different polynomial sketches along with their complex-to-real extensions for $D \in \{2d, 4d\}$. The target polynomial kernel is $(\frac{1}{a} \mathbf{x}^\top \mathbf{y} + 1)^3$ and the data is min-max-scaled. The y-axis is shown in log-scale.

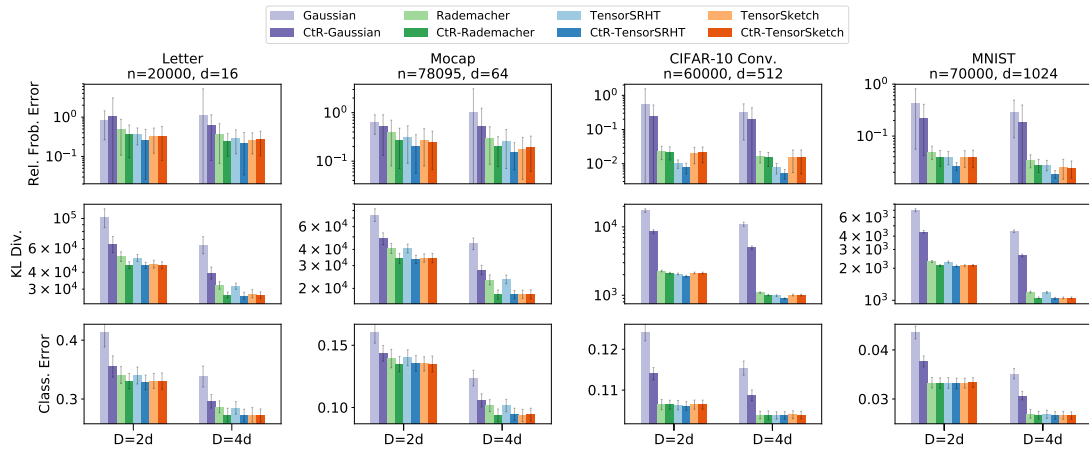


Figure 14. Gaussian Process classification experiments comparing different polynomial sketches along with their complex-to-real extensions for $D \in \{2d, 4d\}$. The target polynomial kernel is $(\frac{1}{a} \mathbf{x}^\top \mathbf{y} + 1)^6$ and the data is min-max-scaled. The y-axis is shown in log-scale.